Chelate Bite Effects for [Pd(triphosphine)(solvent)]$(BF_4)_2$ Complexes in Electrochemical CO_2 Reduction and the Heterolytic Cleavage of Molecular Hydrogen

Sheryl A. Wander,[†] Alex Miedaner,[†] Bruce C. Noll,[‡] Robert M. Barkley,[‡] and Daniel L. DuBois*,[†]

National Renewable Energy Laboratory, Golden, Colorado 80401, and Department of Chemistry and Biochemistry, University of Colorado, Boulder, Colorado 80309

Received February 5, 1996[⊗]

A series of [Pd(triphosphine)(CH_3CN)]$(BF_4)_2$ complexes has been prepared with different chelate bites. Stoichiometric reactions of these complexes with triethylphosphine, $NaBH_4$, and H_2 have been studied, as well as the catalytic electrochemical reduction of CO_2. All of these reactions show significant chelate effects. [Pd(ttpE)(CH_3CN)]$(BF_4)_2$ (where ttpE is bis(3-(diethylphosphino)propyl)phenylphosphine) catalyzes the electrochemical reduction of CO_2 to CO in acidic dimethylformamide solutions and reacts with $NaBH_4$ or H_2 to form [Pd(ttpE)(H)](BF_4). The latter complex is the decomposition product formed under catalytic conditions. X-ray diffraction studies of [Pd(ttpE)(CH_3CN)]$(BF_4)_2$ and [Pd(ttpE)(H)](BF_4) provide insight into possible steric origins of reactivity differences between the last two complexes and analogous complexes with smaller chelate bites. [Pd(ttpE)(CH_3CN)]$(BF_4)_2$ has a square-planar structure with one methylene group of the ethyl substituents making a close contact with the nitrogen atom of acetonitrile. This steric interaction likely contributes to some of the reactivity differences observed. [Pd(ttpE)(H)](BF_4) also has a square-planar structure with the two terminal phosphorus atoms of the triphosphine ligand distorted slightly toward the hydride ligand. Extended Hückel molecular orbital calculations suggest that small chelate bites shift electron density onto the hydride ligand, making it more hydridic, while larger chelate bites shift electron density away from the hydride ligand, making it more acidic.

Introduction

For bidentate phosphine ligands there are numerous examples in which the chelate bite has a major effect on the structure and reactivity of transition-metal complexes. For example, many square-planar d^8 [M(diphosphine)$_2$]$^{2+}$ and [MCl_2(diphosphine)] complexes exhibit tetrahedral distortions.[1,2] This distortion is larger for complexes with large chelate bites and has been attributed to both steric and electronic effects. Regardless of its origin, this distortion results in a lower energy for the LUMO, which is reflected in more positive reduction potentials for complexes with large chelate bites.[3] Differences in reactivity as a function of the chelate bite size have been observed for a number of stoichiometric and catalytic reactions. The insertion of ethylene into the Pt−H bond in [Pt(diphosphine)(ethylene)(H)]$^+$ complexes (where diphosphine = $Bu^t_2P(CH_2)_nPBu^t_2$, n = 2, 3) has been shown to favor an agostic ethyl complex for n = 3 and the hydrido ethylene complex for n = 2.[4] This result is consistent with molecular orbital calculations by Thorn and Hoffmann, suggesting that alkyl formation would be favored by P−Pt−P angles larger than 90°.[5] Similar conclusions have been reached for the insertion of carbon monoxide into M−C bonds of [M(diphosphine)(CH_3)(CO)]$^+$ intermediates (where M = Pt, Pd) based on both experimental data and theoretical analyses.[6,7] The insertion of olefins into Pd−aryl bonds is another reaction that exhibits significant chelate effects.[8] A final and potentially practical example is the use of bidentate ligands with large bite sizes to control the regioselectivity of hydroformylation reactions.[9]

For metal complexes with tridentate and tetradentate phosphine ligands, much less is known about the relationship between the chelate bite size of the ligand and the structure and reactivity of the metal complexes.

[†] National Renewable Energy Laboratory.
[‡] University of Colorado.
[⊗] Abstract published in *Advance ACS Abstracts*, July 1, 1996.

(1) (a) Hall, M. C.; Kilbourn, B. T.; Taylor, K. A. *J. Chem. Soc. A* **1970**, 2539. (b) Anderson, M. P.; Pignolet, L. H. *Inorg. Chem.* **1981**, *20*, 4101. (c) Jones, R. A.; Real, F. M.; Wilkinson, G.; Galas, A. M. R.; Hursthouse, M. B.; Malik, K. M. A. *J. Chem. Soc., Dalton Trans.* **1980**, 511. (d) Marder, T. B.; Williams, I. D. *J. Chem. Soc., Chem. Commun.* **1987**, 1478. (e) Clark, G. R.; Skelton, B. W.; Waters, T. N. *Acta Crystallogr., Sect. C* **1987**, *C43*, 1708. (f) Mercier, F.; Mathey, F.; Fischer, J.; Nelson, J. H. *J. Am. Chem. Soc.* **1984**, *106*, 425.

(2) (a) van Hecke, G. R.; Horrocks, W. D., Jr. *Inorg. Chem.* **1966**, *5*, 1968. (b) McPhail, A. T.; Komson, R. C.; Engel, J. F.; Quin, L. D. *J. Chem. Soc., Dalton Trans.* **1972**, 874. (c) Palenik, G. J.; Mathew, M.; Steffen, W. L.; Bevan, G. *J. Am. Chem. Soc.* **1975**, *97*, 1059. (d) Steffen, W. L.; Palenik, G. J. *Inorg. Chem.* **1976**, *15*, 2432.

(3) Miedaner, A.; Haltiwanger, R. C.; DuBois, D. L. *Inorg. Chem.* **1991**, *30*, 417.

(4) Mole, L.; Spencer, J. L.; Carr, N.; Orpen, A. G. *Organometallics* **1991**, *10*, 49.

(5) Thorn, D. L.; Hoffmann, R. *J. Am. Chem. Soc.* **1978**, *100*, 2079.

(6) (a) Dekker, G. P. C. M.; Elsevier, C. J.; Vrieze, K.; van Leeuwen, P. W. N. M. *Organometallics* **1992**, *11*, 1598. (b) Tóth, I.; Elsevier, C. J. *J. Am. Chem. Soc.* **1993**, *115*, 10388. (c) Tóth, I.; Kégl, T.; Elsevier, C. J.; Kollár, L. *Inorg. Chem.* **1994**, *33*, 5708. (d) Scrivanti, A.; Botteghi, C.; Toniolo, L.; Berton, A. *J. Organomet. Chem.* **1988**, *344*, 261.

(7) Sakaki, S.; Kitaura, K.; Morokuma, K.; Ohkubo, K. *J. Am. Chem. Soc.* **1983**, *105*, 2280.

(8) (a) Portnoy, M.; Ben-David, Y.; Rousso, I.; Milstein, D. *Organometallics* **1994**, *13*, 3465. (b) Portnoy, M.; Ben-David, Y.; Milstein, D. *Organometallics* **1993**, *12*, 4734. (c) Portnoy, M.; Milstein, D. *Organometallics* **1993**, *12*, 1655.

S0276-7333(96)00072-6 CCC: $12.00

In this paper we describe some observations for palladium triphosphine complexes that have arisen during our studies of electrochemical CO_2 reduction. It has been shown that [Pd(triphosphine)(CH_3CN)](BF$_4$)$_2$ complexes will catalyze the electrochemical reduction of CO_2 to CO in acidic acetonitrile or dimethylformamide solutions.[10,11] Two decomposition products were characterized by spectroscopic and X-ray diffraction studies and shown to be Pd(I) dimers with bridging triphosphine ligands, i.e., structures **1a** and **1b**. Presumably, part

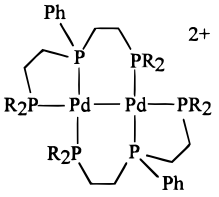

	R
1a	Et
1b	Ph

of the driving force for formation of these dimers is the release of ring strain in reduced catalytic intermediates. On the basis of mechanistic studies, the rate-determining step under normal catalytic conditions is the reaction of a Pd(I) monomeric species with CO_2. Because monomeric Pd(I) complexes would be expected to undergo tetrahedral distortions, a significant amount of strain would result in these complexes, which contain two fused five-membered rings. This strain could be relieved by forming dimers such as **1**. This suggested that dimer formation might be retarded by using triphosphine ligands with a trimethylene linkage between the central and terminal phosphorus atoms. The Pd(I) intermediates formed should be more stable because the six-membered rings could more readily accommodate tetrahedral distortions. If this line of reasoning is correct, then using triphosphine ligands with trimethylene bridges could prevent or retard dimer formation and enhance catalyst lifetime.

In this paper, the synthesis and characterization of [Pd(triphosphine)(CH_3CN)](BF$_4$)$_2$ complexes are described in which the number of methylene groups bridging the phosphorus atoms of the triphosphine ligand is varied in a systematic fashion. This has led to the identification of a new degradation pathway for some of these complexes in which stable palladium hydrides are formed and the discovery of a subtle change in the reaction mechanism during catalytic electrochemical reduction of CO_2. Interesting new reactions in which hydrogen is activated by heterolytic cleavage have also been observed and found to depend markedly on the chelate bite size. In addition, the ligand occupying the fourth coordination site of [Pd(triphosphine)L](BF$_4$)$_2$ complexes is more labile for complexes containing three bridging methylene groups compared to those containing two methylene groups. Possible reasons for some of these chelate effects are explored, based on structural data and qualitative molecular orbital calculations.

Results

Synthesis and Characterization of Ligands. To compare the effect of chelate bite on the chemistry and structure of palladium triphosphine complexes, ligands were needed with different numbers of methylene groups connecting the three phosphorus atoms, i.e., $R_2P(CH_2)_nP(R')(CH_2)_mPR''_2$ (where R, R′, and R″ are alkyl or aryl groups and n and m are 1−3). The free-radical synthesis of etpE (where R = R″ = Et, R′ = Ph, and $n = m = 2$) from divinylphenylphosphine and diethylphosphine has been described elsewhere.[10a] This synthetic method provided a convenient route to a variety of symmetric triphosphine ligands containing two-carbon backbones. Efforts to extend this approach to the synthesis of trimethylene linkages were unsuccessful, as a similar reaction between diallylphenylphosphine and diethylphosphine resulted in the formation of less than 5% of the desired ligand ttpE (**2**), on the basis of ^{31}P NMR spectra of the crude product. Apparently, the presence of two allyl groups leads to undesirable side reactions. However, **2** is readily prepared in moderate yield from phenylphosphine and allyldiethylphosphine using the free-radical-catalyzed route shown in eq 1.[12] Purification of **2** can be accomplished by

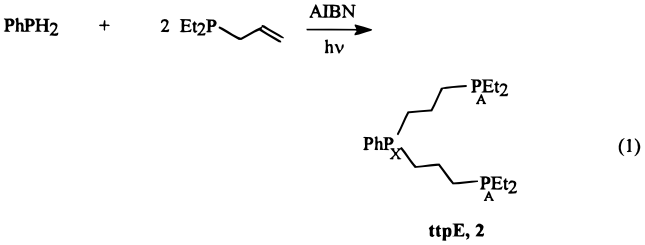

(1)

ttpE, 2

vacuum distillation. The product is a viscous, yellow, air-sensitive oil. The ligand ttpC (**3**), in which the terminal ethyl groups of **2** are replaced with cyclohexyl substituents, was prepared in a strictly analogous fashion. These reactions provide access to ligands with three-carbon backbones.

Reaction of a 4-fold molar excess of $PhPH_2$ with vinyldiethylphosphine forms $Et_2PCH_2CH_2P(H)Ph$ (**4**), which can be converted to the asymmetric triphosphine eptpE (**5**) by a second free-radical-catalyzed reaction with allyldiethylphosphine (eq 2). The synthesis of **5** was designed in this order so that **4** could also be used as an intermediate in the preparation of metpE (**6**); however, the order of P−H addition may be reversed to go via the propylene intermediate $Et_2PCH_2CH_2CH_2P(H)Ph$. The ligand metpE (**6**) was synthesized by reacting the lithium salt of **4**, $Et_2PCH_2CH_2PPh^-Li^+$, with (chloromethyl)diphenylphosphine (eq 3). Ph_2PCH_2Cl was prepared by a method described by Stelzer and

(9) (a) Billig, E.; Abatjoglou, A. G.; Bryant, D. R. (Union Carbide) U.S. Patent 4,769,498, 1988. (b) Hughes, O. R.; Unruh, J. D. *J. Mol. Catal.* **1981**, *12*, 71. (c) Casey, C. P.; Petrovich, L. M. *J. Am. Chem. Soc.* **1995**, *117*, 6007. (d) Casey, C. P.; Whiteker, G. T.; Melville, M. G.; Petrovich, L. M.; Gavney, J. A., Jr.; Powell, D. R. *J. Am. Chem. Soc.* **1992**, *114*, 5535. (e) Moasser, B.; Gladfelter, W. L.; Roe, D. C. *Organometallics* **1995**, *14*, 3832. (f) Kranenburg, M.; van der Burgt, Y. E. M.; Kamer, P. C. J.; van Leeuwen, P. W. N. M.; Goubitz, K.; Fraanje, J. *Organometallics* **1995**, *14*, 3081.

(10) (a) DuBois, D. L.; Miedaner, A.; Haltiwanger, R. C. *J. Am. Chem. Soc.* **1991**, *113*, 8753. (b) DuBois, D. L.; Miedaner, A. *J. Am. Chem. Soc.* **1987**, *109*, 113.

(11) (a) Bernatis, P. R.; Miedaner, A.; Haltiwanger, R. C.; DuBois, D. L. *Organometallics* **1994**, *13*, 4835. (b) Herring, A. M.; Steffey, B. D.; Miedaner, A.; Wander, S. A.; DuBois, D. L. *Inorg. Chem.* **1995**, *34*, 1100. (c) Steffey, B. D.; Miedaner, A.; Maciejewski-Farmer, M.; Bernatis, P. R.; Herring, A. M.; Allured, V.; Caperos, V.; DuBois, D. L. *Organometallics* **1994**, *13*, 4844.

(12) The closely related ligand $PhP(CH_2CH_2CH_2PMe_2)_2$ has been reported: Arpac, E.; Dahlenburg, L. *Angew. Chem., Int. Ed. Engl.* **1982**, *21*, 931.

Table 1. ^{31}P NMR Spectral Data for Ligands and Complexes[a]

	δ (ppm)				J (Hz)					
compd	P_A	P_B	P_X	P_Y or H	J_{AB}	J_{AX}	J_{AY}	J_{BX}	J_{BY}	J_{XY}
ttpE (**2**)	−24.4 (s) [−26]		−26.4 (s) [−28]			0				
ttpC (**3**)	−6.6 (s) [−10]		−26.8 (s) [−28]			0				
eptpE (**5**)	−21.5 (d) [−20]	−24.4 (s) [−26]	−18.8 (d) [−22]			23		0		
metpE (**6**)	−18.6 (d) [−20]	−21.4 (d) [−24]	−25.5 (dd) [−28]			20		118		
Pd(ttpE)$(NCCH_3)^{2+}$ (**7a**)	−0.6 (d)		8.7 (t)			25				
Pd(ttpE)$(PEt_3)^{2+}$ (**7b**)	−5.8 (dd)		−13.3 (dt)	8.2 (dt)		32	36			315
Pd(ttpE)$(H)^+$ (**7c**)	11.4 (d)		−11.2 (t)	−5.0 (d)[b]		43				200[c]
Pd(ttpC)$(CH_3CN)^{2+}$ (**8a**)	10.4 (d)		12.6 (t)			22				
Pd(ttpC)$(H)^+$ (**8c**)	27.4 (d)		−8.5 (t)	−5.1 (d)[b]		40				200[c]
Pd(eptpE)$(NCCH_3)^{2+}$ (**9a**)	76.0 (d)	3.6 (dd)	61.8 (d)		321	0		35		
Pd(eptpE)$(PEt_3)^{2+}$ (**9b**)	68 (dd)	−5 (ddd)	50 (dd)	12 (ddd)	307	0	29	47	25	307
Pd(eptpE)$(H)^+$ (**9c**)	65.3 (dd)	17.3 (dd)	40.3 (dd)	−3.7 (d)[b]	327	21		43		206[c]
Pd(etpE)$(NCCH_3)^{2+}$ (**10a**)[d]	61.9 (d)		114.1 (t)			7				
Pd(etpE)$(PEt_3)^{2+}$ (**10b**)[d]	55.9 (dd)		115.5 (dt)	10.0 (dt)		12	30			303
Pd(etpC)$(NCCH_3)^{2+}$ (**11a**)[d]	74.5 (d)		115.6 (t)			4				
Pd(etpC)$(PEt_3)^{2+}$ (**11b**)	77.1 (m)		120.4 (m)	7.7 (dt)		<10	30			300
Pd(etpC)$(H)^+$ (**11c**)	71.2 (d)		93.1 (t)	−2.9 (d)[b]		16				213[c]
Pd(metpE)$(NCCH_3)^{2+}$ (**12a**)[e]	87 (d)	−44.3 (d)	49.7 (m)		230					
Pd(metpE)$(PEt_3)^{2+}$ (**12b**)[e]	73 (dd)	−49.4 (ddd)	29.5 (dd)	18.4 (ddd)	281	0	26	47	17	320

[a] All ligand spectra were recorded in toluene-d_8. All spectra for the metal complexes were recorded in CD_3CN, with the exception of the triethylphosphine complexes, which were recorded in CD_2Cl_2 or CD_3NO_2. [b] Hydride resonance observed in ^{1}H NMR. [c] P−H coupling constant between the hydride and the central phosphorus atom of the triphosphine ligand. [d] Data taken from ref 10a. [e] A dimeric species is also present in solution. See text for discussion.

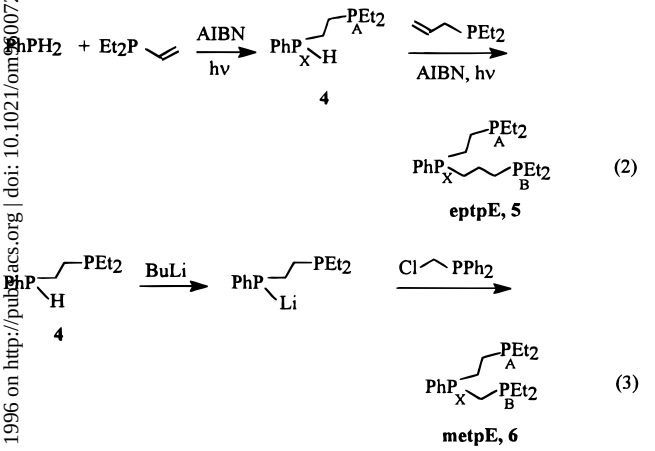

(2)

(3)

co-workers that involves the phase-transfer-catalyzed alkylation of Ph_2PH with CH_2Cl_2 in dichloromethane/toluene/water.[13] Attempts to prepare Et_2PCH_2Cl in an analogous manner were unsuccessful because Et_2PH is unreactive under these conditions.

^{31}P NMR data listed in Table 1 support the structures assigned to the ligands **2**−**6**. The calculated values for the chemical shifts (shown in brackets in Table 1) are in reasonable agreement with the experimentally observed values.[14] For ttpE (**2**) and ttpC (**3**), two singlets are observed with integration ratios of 2:1 for the resonances of the terminal phosphorus atoms compared to the resonances of the central phosphorus atoms. No P−P coupling is observed for these two ligands. Other triphosphine ligands containing trimethylene linkages exhibit either small or no P−P coupling.[12,15] For the unsymmetrical ligands eptpE (**5**) and metpE (**6**), three resonances are observed for the three different phosphorus atoms. For eptpE, no coupling is observed through the trimethylene bridge, consistent with the results for ttpE and ttpC. A 23 Hz coupling is observed between nuclei A and X of eptpE, which is consistent with the three-bond couplings observed for a variety of other triphosphine ligands with ethylene linkages.[10,11] A similar coupling is observed between nuclei A and X for metpE, but the two-bond coupling between B and X is much larger (118 Hz), as expected on the basis of related compounds.[13b] Compound **4** exhibits a doublet in the proton-coupled ^{31}P NMR spectrum due to P−H coupling ($^1J_{PH}$ = 204 Hz).

Synthesis and Characterization of Metal Complexes. Reaction of the tridentate ligands ttpE, ttpC, and eptpE with $[Pd(NCCH_3)_4](BF_4)_2$ provides a convenient route to complexes of the type [Pd(triphosphine)$(CH_3CN)](BF_4)_2$, as shown in eq 4. The same method

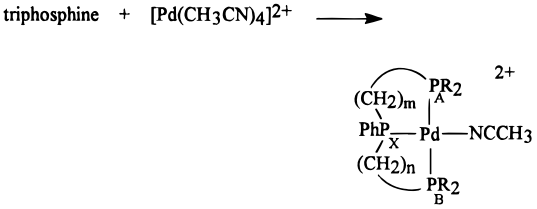

(4)

	m	n	R	L
7a	3	3	Et	ttpE
8a	3	3	Cy	ttpC
9a	2	3	Et	eptpE
10a	2	2	Et	etpE
11a	2	2	Cy	etpC

has been used previously to prepare [Pd(etpE)$(CH_3CN)](BF_4)_2$ and [Pd(etpC)$(CH_3CN)](BF_4)_2$.[10] The new complexes are pale yellow solids, stable to oxygen, and are somewhat hygroscopic. They have been characterized by ^{1}H and ^{31}P NMR spectroscopy, IR spectroscopy, cyclic voltammetry, and elemental analyses. [Pd(ttpE)$(CH_3CN)](BF_4)_2$ has also been characterized by X-ray crystallography, as discussed below.

The ^{31}P NMR spectra of these complexes are summarized in Table 1. The spectra of [Pd(ttpE)$(CH_3CN)]$-

(13) (a) Langhans, K.-P.; Stelzer, O.; Weferling, N. *Chem. Ber.* **1990**, *123*, 995. (b) Langhans, K.-P.; Stelzer, O. *Chem. Ber.* **1987**, *120*, 1707.

(14) Fluck, E.; Heckmann, G. In *Phosphorus-31 NMR Spectroscopy in Stereochemical Analysis*; Verkade, J. G., Quin, L. D., Eds.; Methods in Stereochemical Analysis 8; VCH: Deerfield Beech, FL, 1987; pp 88−93.

(15) (a) Green, L. M.; Meek, D. W. *Polyhedron* **1990**, *9*, 35. (b) Baacke, M.; Hietkamp, S.; Morton, S.; Stelzer, O. *Chem. Ber.* **1981**, *114*, 2568.

$(BF_4)_2$ and $[Pd(ttpC)(CH_3CN)](BF_4)_2$ each consist of a doublet and triplet for the terminal and central phosphorus atoms, respectively. The chemical shifts and coupling constants are typical of phosphorus atoms bound to palladium in six-membered rings.[15,16] The spectrum of $[Pd(eptpE)(NCCH_3)]^{2+}$ consists of two doublets and a doublet of doublets. The doublet of doublets is assigned to the terminal phosphorus atom, P_B, which is in the six-membered ring. The strong trans coupling constant of 321 Hz is consistent with either P_A or P_B, but its chemical shift (3.6 ppm) is similar to that of the terminal phosphorus atom of $[Pd(ttpE)(CH_3CN)](BF_4)_2$. P_A is shifted much further downfield (76 ppm) due to the five-membered-ring effect[16] and has a large trans coupling. The remaining resonance is assigned to the central phosphorus atom, P_X, with the doublet structure arising from the cis coupling to P_B.

The products of the reaction of $[Pd(CH_3CN)_4](BF_4)_2$ with metpE are solvent- and temperature-dependent. At room temperature, two isomers are formed in acetonitrile, which we propose are a monomer, $[Pd(metpE)(NCCH_3)]^{2+}$ (**12a**), and a dimer, $[Pd(metpE)(NCCH_3)]_2^{4+}$ (**13a**), in equilibrium (eq 5). When the solution is

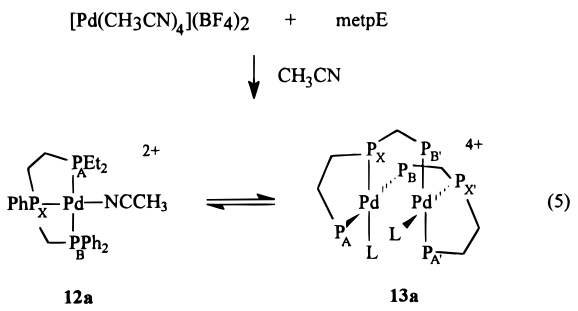

12a **13a** (5)

warmed to 60 °C, only the resonances assigned to the monomer are observed. When it is cooled to −35 °C, only resonances assigned to the dimer are observed. The ^{31}P NMR spectrum of monomer **12a** has a doublet at 44.3 ppm (P_B). This chemical shift is diagnostic of a coordinated phosphorus atom in a four-membered ring.[16] The large splitting of 230 Hz, while smaller than the trans couplings described above, requires a trans arrangement with respect to P_A. The latter resonance has a large downfield shift (87 ppm) due to its incorporation in a five-membered ring. The remaining resonance at 49.7 ppm is an unresolved multiplet, and it is assigned to P_X. Similarly, three resonances are also assigned to dimer **13a**. In this case, the resonance for the diphenylphosphino group, P_B, occurs at 9.3 ppm, consistent with incorporation into a larger eight-membered ring. In addition to smaller coupling to P_X and $P_{X'}$, P_B exhibits a strong doublet splitting of 347 Hz (N_{AB}) due to the trans phosphine ligand, P_A. The chemical shift of the doublet for P_A occurs at 98.6 ppm, consistent with incorporation in a five-membered ring. The experimental and simulated spectra of **13a** are shown in Figure 1. Dimer **13a** is one of three possible isomers and has a cis arrangement of the two PCH_2P bridges. Dimers **13b** and **13c** have trans PCH_2P bridges, with the solvent molecule binding on either the same side or opposite sides of the plane formed by the two diphosphine bridges. Dimer **13a** is the only dimer observed in

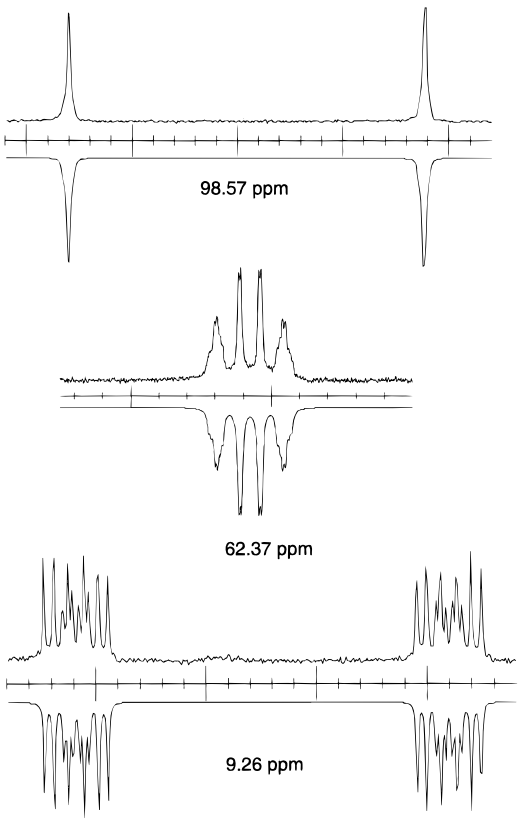

Figure 1. Experimental (upward) and calculated (downward) ^{31}P NMR spectra for isomer **13a**. Parameters used in the simulation are listed in the Experimental Section. Each minor division represents 20 Hz.

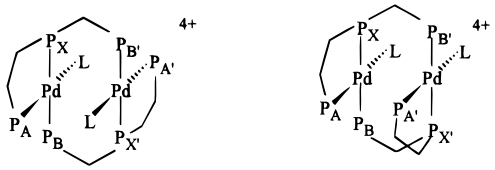

13b **13c**

acetonitrile. In acetone solutions containing approximately 5% acetonitrile, three isomers are observed, as indicated by three separate resonances for the diethylphosphino group, P_A (98.6, 86.4, and 85.3 ppm). As might be expected, there is significant spectral overlap for resonances attributed to P_M and P_X and a complete spectral analysis of the three overlapping AA′MM′XX′ spectra was not attempted. Redissolution of material isolated from acetone solutions with no excess acetonitrile contained only one dimer, **13b** or **13c**, which have trans bridging groups and acetone as the solvent ligand. Simulated and experimental spectra for this isomer are given in Figure 3s of the Supporting Information, and the parameters used in the simulation are listed in the Experimental Section. Although satisfactory analytical data were obtained for the material isolated from the reaction of $[Pd(CH_3CN)_4](BF_4)_2$ with metpE, crystals suitable for X-ray diffraction studies were not obtained, perhaps due to the number of isomers and equilibria involving solvent molecules. However, the ^{31}P NMR spectral data under different conditions are unambiguous in demonstrating the existence of various isomers of **13** and a monomer−dimer equilibrium in acetonitrile.

Triethylphosphine Complexes. The acetonitrile ligands in complexes **7a**−**12a** and **13** are labile. This

(16) Garrou, P. E. *Chem. Rev.* **1981**, *81*, 229.

lability is demonstrated by the observation that the addition of small amounts of acetonitrile to solutions of [Pd(triphosphine)(CH_3CN)](BF_4)$_2$ in acetone-d_6 or CD_2Cl_2 results in a shift of the resonance of coordinated acetonitrile toward the position of free acetonitrile. Advantage can be taken of the lability of the acetonitrile ligand to replace it with monodentate phosphine ligands or hydrides. Reaction of **7a** and **9a**−**11a** with triethylphosphine readily forms the corresponding [Pd(triphosphine)(PEt_3)](BF_4)$_2$ complexes. The ^{31}P NMR spectra for these complexes are summarized in Table 1. In comparison to the corresponding acetonitrile complexes, the triethylphosphine complexes exhibit new resonances assigned to the triethylphosphine ligands with chemical shifts ranging from 8 to 18 ppm. These resonances display large trans couplings between 305 and 320 Hz. The resonances assigned to the tridentate ligand in these complexes show an additional splitting compared to their corresponding acetonitrile complexes due to the presence of coordinated triethylphosphine. Because complex **12a** exists in equilibrium with **13a** (eq 5), it is not surprising that two products are formed in this reaction. The major product is monomeric [Pd(metpE)(PEt_3)]$^{2+}$ (**12b**; ∼75%), while minor components appear to be the triethylphosphine adducts of **13a**, **13b**, and **13c** (∼25%). In the case of [Pd(ttpC)(CH_3CN)](BF_4)$_2$, which contains bulky cyclohexyl terminal substituents, no reaction is observed with triethylphosphine even in noncoordinating solvents such as acetone. In contrast, the two-carbon-chain analogue [Pd(etpC)(CH_3CN)](BF_4)$_2$ reacts readily to form [Pd(etpC)(PEt_3)](BF_4)$_2$. The three-carbon linkage in the ttpC ligand decreases the stability of the triethylphosphine complex compared to its two-carbon analogue. The origin of this difference is discussed in more detail below.

Metal Hydride Complexes. The hydride complexes [Pd(ttpE)(H)]$^+$, [Pd(ttpC)(H)]$^+$, [Pd(eptpE)(H)]$^+$, and [Pd(etpC)(H)] (**7c**, **8c**, **9c**, and **11c**, respectively) can be prepared from their corresponding acetonitrile complexes by reaction with $NaBH_4$ on alumina. The ^{31}P NMR spectra (Table 1) of these complexes are similar to those of their acetonitrile analogues. The ^{1}H NMR spectra exhibit broad doublets between −2 and −6 ppm with $^2J_{PH}$ values of approximately 200 Hz (see Table 1). These values are similar to those observed previously for [Pd(ttp)(H)](BF_4)[10] (where ttp is bis(3-(diphenylphosphino)propyl)phenylphosphine). In addition, weak Pd−H stretches are observed for Nujol mulls of each complex (1830, 1864, and 1896 cm^{-1} for **7c**, **8c**, and **9c**, respectively).

For [Pd(etpE)(CH_3CN)](BF_4)$_2$, a complex mixture of products is formed upon reaction with $NaBH_4$ on alumina. Reaction of [Pd(metpE)(CH_3CN)]$^{2+}$ with $NaBH_4$ produces a Pd(I) dimer, [Pd(metpE)]$_2^{2+}$ (**14**),

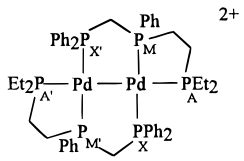

14

quantitatively by ^{31}P NMR. No evidence of a hydride is observed. Two isomers of **14** are expected due to the chiral phosphorus atoms P_M. Selective precipitation from a dichloromethane/ethanol mixture produces predominantly one isomer, but the separation is not complete. The analytical data, however, are satisfactory as expected for isomeric impurities. The ^{31}P NMR spectrum of [Pd(metpE)]$_2$(BF_4)$_2$ is consistent with an AA′MM′XX′ spin system. The resonance for P_X is observed at −8.8 ppm, compared to a chemical shift of −5.9 ppm for the bridging dppm ligand in [Pd(dppm)(CH_3CN)]$_2$(BF_4)$_2$ (dppm is bis(diphenylphosphino)methane).[17] This resonance has a large splitting (N_{MX} = 420 Hz) that is largely due to the trans coupling to P_M (35.0 ppm). The resonance for P_A is a complex multiplet at 52.5 ppm. A FAB mass spectrum of the tetrafluoroborate salt of **14** exhibits strong ion peaks at *m*/*z* 1149 and 1061 consistent with loss of BF_4^- and $H(BF_4)_2^-$ anions, respectively. These peaks have appropriate isotopic ratios for two palladium atoms.

The hydrides [Pd(ttpE)(H)]$^+$ (**7c**) and [Pd(ttpC)(H)]$^+$ (**8c**) can also be formed by direct reaction of **7a** and **8a** with 1 atm of hydrogen at room temperature in dimethylformamide or acetone solution, as shown in eq 6. This reaction is reversible for **7a**. Addition of HBF_4

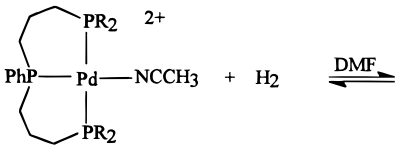

R	
7a	Et
8a	Cy

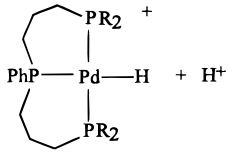

(6)

R	
7c	Et
8c	Cy

to dimethylformamide solutions of **7c** results in the formation of a mixture of **7a**, **7c**, and hydrogen (detected by ^{1}H NMR spectroscopy and gas chromatography). The forward and reverse reactions shown in eq 6 have half-lives of approximately 1.5 h. For the cyclohexyl analogue **8c**, the equilibrium appears to lie farther to the right. Reaction 6 is observed only for complexes containing triphosphine ligands with two trimethylene linkages. No reaction is observed for [Pd(eptpE)(CH_3CN)]$^{2+}$ (**9a**) or [Pd(etpE)(CH_3CN)]$^{2+}$ (**10a**), which contain one and two ethylene linkages, respectively.

Structural Studies. X-ray diffraction studies were carried out on [Pd(ttpE)(CH_3CN)](BF_4)$_2$ and [Pd(ttpE)(H)](BF_4) to obtain insight into structural features that play a role in the reactivity and stability of these complexes. Crystals of [Pd(ttpE)(CH_3CN)](BF_4)$_2$ were grown from a mixture of dichloromethane and ethanol and consist of [Pd(ttpE)(CH_3CN)]$^{2+}$ cations, BF_4^- anions, and molecules of dichloromethane. A drawing illustrating the structure and atom-numbering scheme for the cation is shown in Figure 2. Selected bond

(17) Miedaner, A.; DuBois, D. L. *Inorg. Chem.* **1988**, *27*, 2479.

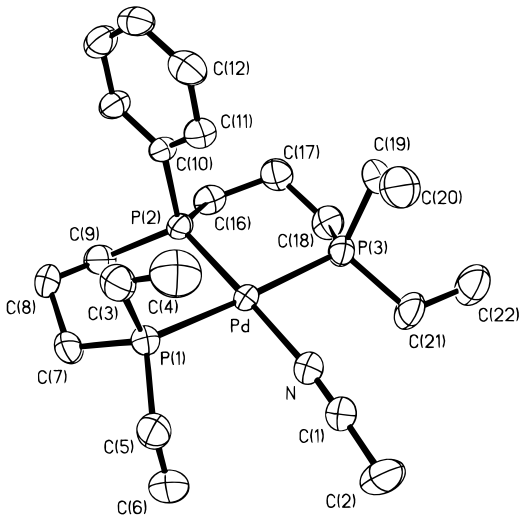

Figure 2. Thermal ellipsoid drawing of the cation [Pd(ttpE)(CH_3CN)]$^{2+}$ (**7a**) at the 50% probability level showing the atom-numbering scheme. Hydrogen atoms have been omitted for clarity.

Table 2. Selected Bond Distances (Å) and Bond Angles (deg) for [Pd(ttpE)(CH_3CN)]$^{2+}$ (7a) and [Pd(ttpE)(H)]$^+$ (7c)

7a		7c	
	Bond Distances		
Pd−N	2.071(6)	Pd−H(1)	1.64(3)
Pd−P(1)	2.393(2)	Pd−P(1)	2.2815(8)
Pd−P(2)	2.264(2)	Pd−P(2)	2.2923(7)
Pd−P(3)	2.383(2)	Pd−P(3)	2.2751(8)
N−C(1)	1.140(8)		
C(1)−C(2)	1.471(10)		
	Bond Angles		
P(2)−Pd−P(1)	178.5(2)	H(1)−Pd−P(2)	177.2(10)
P(3)−Pd−P(1)	88.8(2)	H(1)−Pd−P(1)	86.1(10)
P(2)−Pd−P(3)	90.5(2)	H(1)−Pd−P(3)	87.0(10)
P(2)−Pd−P(1)	89.75(6)	P(2)−Pd−P(1)	92.83(4)
P(2)−Pd−P(3)	90.96(6)	P(2)−Pd−P(3)	94.05(3)
P(1)−Pd−P(3)	174.23(7)	P(1)−Pd−P(3)	173.10(2)
C(1)−N−Pd	174.0(6)		
N−C(1)−C(2)	178.3(8)		
C(16)−P(2)−Pd	118.3(2)	C(14)−P(2)−Pd	117.87(8)
C(17)−C(16)−P(2)	118.4(5)	C(15)−C(14)−P(2)	114.3(2)
C(18)−C(17)−C(16)	114.1(6)	C(16)−C(15)−C(14)	113.1(2)
C(17)−C(18)−P(3)	114.7(5)	C(15)−C(16)−P(3)	116.9(2)
C(18)−P(3)−Pd	117.1(2)	C(16)−P(3)−Pd	116.23(8)

distances and bond angles are given in Table 2. Crystals of [Pd(ttpE)(H)](BF_4) were grown from a mixture of acetone and ethanol at −20 °C. The crystals consist of [Pd(ttpE)(H)]$^+$ cations and BF_4^- anions. A drawing of the [Pd(ttpE)(H)]$^+$ cation is shown in Figure 3 with the atom-numbering scheme. Selected bond distances and bond angles for this cation are also given in Table 2.

It is useful to compare some structural features of [Pd(ttpE)(CH_3CN)]$^{2+}$ (**7a**) and [Pd(ttpE)(H)]$^+$ (**7c**) with those of the previously studied [Pd(MesetpE)(CH_3CN)]$^{2+}$ (**15**).[11] The bond angles between the terminal and central phosphorus atoms are very close to the ideal value of 90° for **7a** but deviate significantly for **15** (approximately 85°) and **7c** (approximately 93°). Similarly, the P−Pd−N bond angles between the terminal phosphorus atoms and the nitrogen atom of the acetonitrile ligand are about 5° smaller for **7a** compared to **15**, and the P−Pd−H angle of **7c** is approximately 3° smaller than the corresponding P−Pd−N angle in **7a**. The less than 90° P−Pd−P bond angles between the

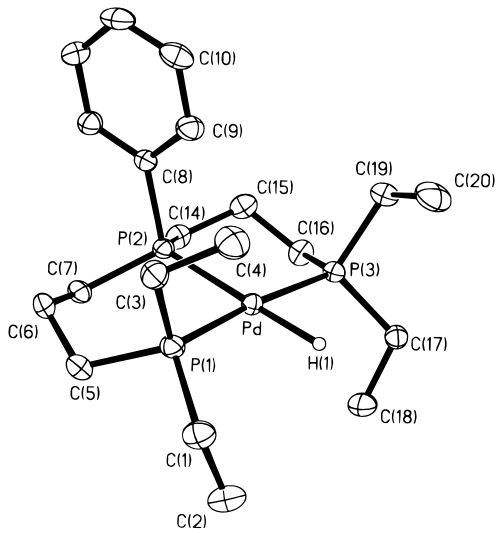

Figure 3. Thermal ellipsoid drawing of the cation [Pd(ttpE)(H)]$^+$ (**7c**) at the 50% probability level showing the atom-numbering scheme. All hydrogen atoms except for the hydride ligand have been omitted for clarity.

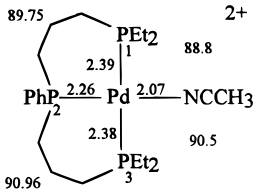

7a

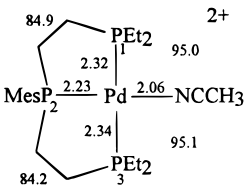

15

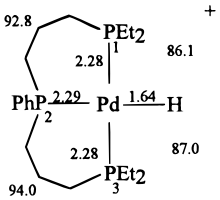

7c

terminal and central phosphorus atoms of **15** can be attributed to steric constraints imposed by the five-membered rings. The bending of the terminal phosphorus atoms of **7c** toward the hydride ligand is a common feature of hydrides and can be attributed to both steric and electronic effects.[18]

The different ring sizes for **15** compared to **7a** and **7c** also have another effect. Figure 4 gives edge-on views of **15** and **7a**, looking down what are nominally the P(1)−Pd−P(3) axes. From this perspective, it can be seen that the P(2)−Pd−N axis of **15** approximately bisects the angle formed by the two ethyl groups of the terminal phosphorus atoms. For **7a**, one of the ethyl groups is almost parallel to the P(2)−Pd−N axis, while the second is slightly less than perpendicular. As a result, one of the ethyl substituents in **7a** is much closer to the acetonitrile ligand than is the case for **15**. As a measure of this interaction, the C(3)−N and C(5)−N distances in **7a** are 4.16 and 3.23 Å, respectively, while the analogous distances in **15** are 3.90 and 3.72 Å, respectively. The 3.23 Å distance between C(3) and N

(18) (a) Elian, M.; Hoffmann, R. *Inorg. Chem.* **1975**, *14*, 1058. (b) Albright, T. A.; Hoffmann, R.; Thibeault, J. C.; Thorn, D. L. *J. Am. Chem. Soc.* **1979**, *101*, 3810.

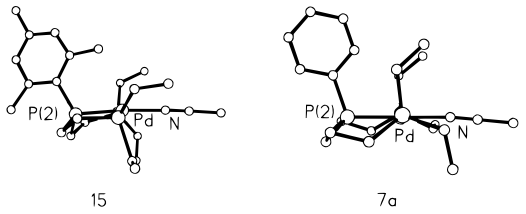

Figure 4. Drawing illustrating the effect of ring size on the positioning of the substituents of the terminal phosphorus atom with respect to the coordinated acetonitrile ligand for $[Pd(MesetpE)(CH_3CN)]^{2+}$ (**15**) and $[Pd(ttpE)(CH_3CN)]^{2+}$ (**7a**).

for **7a** is less than the sum of the van der Waals radii for a methyl group (2.0 Å) and nitrogen (1.5 Å), and this suggests a steric interaction between the substituents on the terminal phosphorus atoms and the fourth ligand in palladium complexes containing triphosphine ligands with trimethylene linkages. The Pd−P bond distances of terminal phosphorus atoms are 0.1 Å longer for **7a** compared to **7c**. The long bond distances of **7a** likely reflect the repulsion between C(3) and N. The repulsion appears to be manifested in the terminal Pd−P bond distances of **7a** and not in the Pd−N bond distance, which is similar to that observed for **15** and other second-row transition-metal complexes of acetonitrile.[19] The lengthening of the Pd−P bonds and not the Pd−N bond may arise from the fact that two methylene groups interacting with the acetonitrile ligand oppose each other. The resulting steric force is perpendicular to the acetonitrile ligand and parallel to the Pd−P bonds. As a result, it is the Pd−P bonds that are lengthened.

The Pd−H bond distances range from 1.46 to 1.79 Å for the relatively few palladium hydrides in which the hydrogen atom has been located by X-ray diffraction studies.[20] The Pd−H distance of 1.64 Å observed for **7c** falls within this range, and it appears normal for other second-row transition metals such as Ru and Rh.[21]

Electrochemical Studies. Triethylphosphine Complexes. Figure 5 shows the cyclic voltammogram of $[Pd(eptpE)(PEt_3)]^{2+}$ (**9**) in dimethylformamide. A single diffusion-controlled, two-electron reduction is observed at −1.30 V vs the ferrocene/ferrocenium couple. A plot of the peak current vs the square root of the scan rate is linear between 0.05 and 1.0 V/s, confirming diffusion control over this range of scan rates. The observed wave has a peak-to-peak separation of 33 mV and an $i_{p,a}/i_{p,c}$ ratio of 0.96 at a scan rate of 20 mV/s. These data are consistent with a reversible two-electron transfer, for which a peak-to-peak separation of 30 mV and an $i_{p,a}/i_{p,c}$ ratio of 1.0 are expected.[22] However, controlled-potential electrolysis of this complex at −1.4 V resulted in the passage of 1.0 faraday/mol of complex, indicating that, on the longer time scale required for bulk electrolysis, a one-electron reduction is observed.

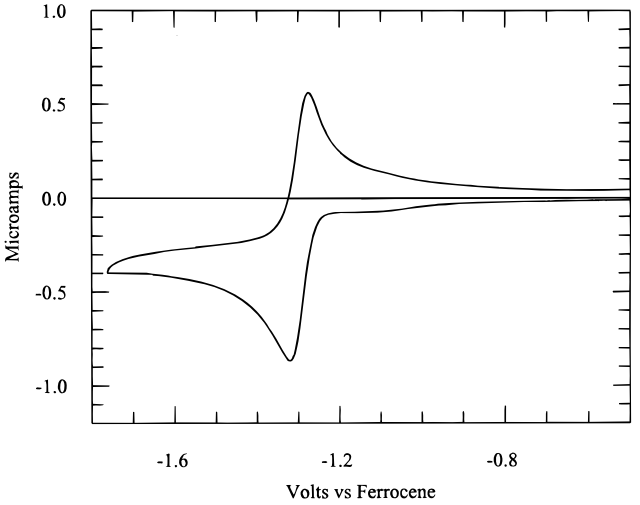

Figure 5. Cyclic voltammogram of 1.0×10^{-3} M $[Pd(eptpE)(PEt_3)](BF_4)_2$ in a dimethylformamide solution containing 0.3 N NBu_4BF_4 at 20 mV/s.

Table 3. Electrochemical Data for [Pd(triphosphine)L](BF$_4$)$_2$ Complexes in Dimethylformamide

complex	$E_{1/2}$[a]	n[b]	current efficiency[c] CO	current efficiency[c] H_2	turnover no.[d]
$[Pd(ttpE)(CH_3CN)](BF_4)_2$	−1.27 (q)	1.0	95	7	120
$[Pd(ttpC)(CH_3CN)](BF_4)_2$	−1.15 (q)	1.1	70	31	3
$[Pd(eptpE)(CH_3CN)](BF_4)_2$	−1.45 (q)	1.4	64	39	83
$[Pd(etpE)(CH_3CN)](BF_4)_2$[e]	−1.25 (i)	1.1	65	37	10
$[Pd(etpC)(CH_3CN)](BF_4)_2$[e]	−1.28 (i)	1.0	97	7	130
$[Pd(ttpE)(PEt_3)](BF_4)_2$	−1.18 (r)	1.2			
$[Pd(eptpE)(PEt_3)](BF_4)_2$	−1.30 (r)	1.0			
$[Pd(etpE)(PEt_3)](BF_4)_2$e	−1.35 (r)	1.9			
$[Pd(etpC)(PEt_3)](BF_4)_2$	−1.33 (r)	1.0			

[a] Potentials are given versus the ferrocene/ferrocenium couple and correspond to the half-wave potential under catalytic conditions for the acetonitrile complexes. The letters in parentheses indicate whether the wave is reversible (r), quasi-reversible (q), or irreversible (i). [b] Number of faradays passed per mole of complex during bulk electrolysis at a potential approximately 0.1 V more negative than the listed $E_{1/2}$ value. Reductions of acetonitrile complexes were carried out under an atmosphere of CO_2. Reductions of triethylphosphine complexes were carried out under nitrogen. [c] Current efficiencies were calculated on the assumption that two electrons are required for CO and H_2 production. [d] Number of moles of CO formed per mole of catalyst after current had decayed to 5−10% of initial value. [e] Data from ref 10a.

Similar experiments were carried out for the complexes $[Pd(ttpE)(PEt_3)](BF_4)_2$ and $[Pd(etpE)(PEt_3)](BF_4)_2$, and the results are summarized in Table 3. In order to obtain a fully reversible wave for $[Pd(ttpE)(PEt_3)](BF_4)_2$, it was necessary to add a 5−10-fold excess of triethylphosphine to retard ligand dissociation. Under these conditions, a reversible two-electron reduction is observed using the criterion of peak-to-peak separation and the ratio of anodic to cathodic currents. Data are not reported for $[Pd(metpE)(PEt_3)](BF_4)_2$, since this compound could not be isolated in pure form as discussed above. It can be seen from the data in Table 3 that increasing the bite size of the tridentate ligand leads to a less negative redox potential for the Pd(II)/Pd(0) couple. This trend is expected since larger chelate bites should produce more stable tetrahedral Pd(0) complexes, which would ideally have P−Pd−P bond angles of 109°.

Acetonitrile Complexes. The cyclic voltammogram

(19) Storkhoff, B. N.; Lewis, H. C., Jr. *Coord. Chem. Rev.* **1977**, *23*, 1.

(20) (a) Bugno, C. D.; Pasquali, M.; Leoni, P.; Sabatino, P.; Braga, D. *Inorg. Chem.* **1989**, *28*, 1390. (b) Leoni, P.; Sommovigo, M.; Pasquali, M.; Midollini, S.; Braga, D.; Sabatino, P. *Organometallics* **1991**, *10*, 1038. (c) Portnoy, M.; Frolow, F.; Milstein, D. *Organometallics* **1991**, *10*, 3960. (d) Fryzuk, M. D.; Lloyd, B. R.; Clentsmith, G. K. B.; Rettig, S. J. *J. Am. Chem. Soc.* **1991**, *113*, 4332.

(21) (a) Fryzuk, M. D.; Jones, T.; Einstein, F. W. B. *Organometallics* **1984**, *3*, 185. (b) Jia, G.; Meek, D. W.; Gallucci, J. *Inorg. Chem.* **1991**, *30*, 403.

(22) Bard, A. J.; Faulkner, L. R. *Electrochemical Methods*; Wiley: New York, 1980; p 218.

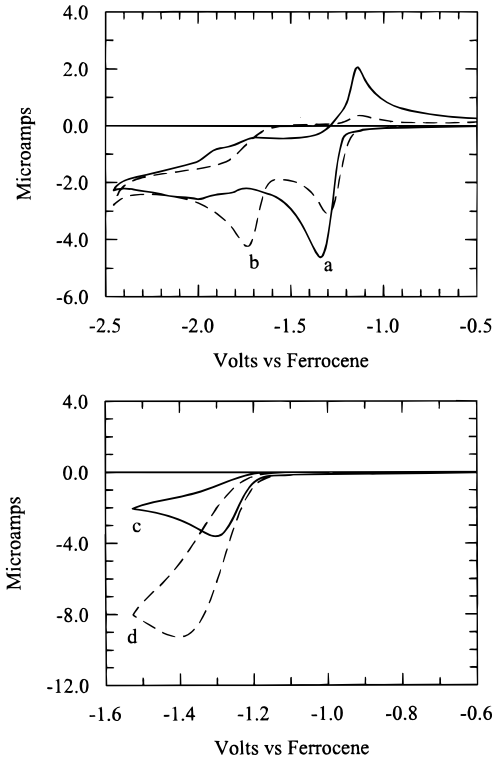

Figure 6. Cyclic voltammograms of dimethylformamide solutions of 2.90×10^{-3} M [Pd(ttpE)(CH_3CN)](BF_4)$_2$ under (a) nitrogen (—) and (b) CO_2 (- - -) and cyclic voltammograms of dimethylformamide solutions containing 2.70×10^{-2} M HBF_4 and 2.30×10^{-3} M [Pd(ttpE)(CH_3CN)](BF_4)$_2$ under (c) nitrogen (—) and (d) CO_2 (- - -).

of [Pd(ttpE)(CH_3CN)]$^{2+}$ (**7a**) shown by the solid line (a) in Figure 6 is typical of the acetonitrile complexes **7a**−**9a** under nitrogen atmospheres. All of the complexes exhibit an irreversible or quasi-reversible cathodic wave between −1.15 and −1.45 V vs the ferrocene/ferrocenium couple. These waves are diffusion-controlled between 0.05 and 1.0 V/s, as indicated by linear plots of peak currents vs the square root of the scan rate. To determine the number of electrons involved in the reduction wave for **7a**, the slopes of chronocoulometric plots of charge vs $t^{1/2}$ were compared for **7a** and **7b**. For such plots, the slope is proportional to the number of electrons involved in the charge-transfer step.[23] In the presence of excess triethylphosphine, a two-electron-reduction process was established for **7b** as discussed above. The observed ratio of the slope of **7a** to **7b** was found to be 0.85, indicating approximately 1.7 faraday/mol of complex is passed during the reduction of **7a**. This value is consistent with the 1.6 faraday/mol of complex observed for bulk electrolysis experiments carried out under nitrogen at −1.4 V. These data suggest that both one- and two-electron processes are occurring during the reduction of **7a**. In the presence of CO_2, the voltammogram shown by the dashed line (b) in Figure 6 is observed. The cathodic wave is decreased in height and shifted in a positive direction, which is consistent with a fast chemical reaction of the reduction product of **7a** with CO_2. The ratio of the slopes of the chronocoulometric plots of the first reduction process for **7a** under CO_2 and **7b** under nitrogen is 0.57. This value corresponds to 1.1 faraday/mol of **7a** assuming a value of 2.0 faraday/mol for **7b**. This result supports a one-electron reduction of **7a** in the presence of CO_2. Bulk electrolysis of **7a** under CO_2 is again consistent with the chronocoulometric results, as 1.0 faraday/mol of palladium complex was consumed. The ^{31}P NMR spectra of the electrolysis products under nitrogen and CO_2 were identical with that observed for [Pd(ttpE)(H)](BF_4). The results show that the hydride **7c** can be formed by either one- or two-electron-reduction pathways. Under an atmosphere of CO_2, only the one-electron pathway is operative, indicating that the Pd(I) complex acts as a radical abstracting a hydrogen atom from the solvent. Under a nitrogen atmosphere, transient Pd(I) and Pd(0) species react to abstract a hydrogen atom or a proton, respectively. In the latter case, the proton is likely obtained from trace amounts of water remaining in the solvent or from the supporting electrolyte. Similarly, [Pd(triphosphine)(H)]$^+$ complexes **8b**, **9b**, and **11b** are formed as the major products during electrochemical reduction of the corresponding [Pd(triphosphine)(CH_3CN)](BF_4)$_2$ complexes in dimethylformamide solutions saturated with CO_2. For [Pd(etpE)(CH_3CN)]$^{2+}$ (**10a**) electrochemical reduction produces dimer **1a** in nearly quantitative yield as reported previously.[10a]

In the presence of CO_2, a second reduction wave is observed for [Pd(ttpE)(CH_3CN)](BF_4)$_2$ as shown in Figure 6 (trace b). This wave may be due to either a Pd^I(CO_2) complex or to [Pd(ttpE)(H)](BF_4), which has a reduction wave at the same potential (within 0.02 V), as verified by cyclic voltammograms of the hydride in the presence of CO_2. Similar results were obtained for the other complexes that form hydrides, which suggests that hydride formation is responsible for the second wave and that the lifetime of the Pd^I(CO_2) complexes is short (less than 0.1 s). In the presence of acid, the Pd^I(CO_2) intermediates undergo further reduction to form CO in a catalytic process, as discussed below.

Catalytic Studies. Cyclic voltammograms of [Pd(ttpE)(CH_3CN)](BF_4)$_2$ in acidic dimethylformamide solutions (0.027 M HBF_4) saturated with nitrogen and CO_2 at 620 mmHg are shown by traces c and d, respectively, of Figure 6. In the presence of CO_2, a current enhancement is observed. To determine the nature of the products formed during the reduction process, a controlled-potential electrolysis of **7a** in the presence of CO_2 and acid was carried out in a sealed cell at −1.4 V. Gas chromatographic analysis of the gases formed during the electrolysis indicated that, initially, approximately 95% of the charge passed resulted in the production of CO, while 7% produced hydrogen. The selectivity for CO gradually decreases with time. Similar experiments were carried out for **8a** and **9a**, and the resulting data are listed in Table 3. A turnover number of 120 was calculated on the basis of the moles of CO produced per mole of catalyst. The catalyst was considered deactivated when the current had decayed to approximately 10% of its initial value. Similar experiments were carried out for other acetonitrile complexes, and the results are presented in Table 3.

The dependence of the catalytic current on substrate and catalyst concentrations is shown in Figures 7 and 8. Plots of the catalytic currents for **7a** and **8a** vs the acid concentration are biphasic (Figure 7, open circles). The catalytic current initially increases with acid con-

(23) Anson, F. C. *Anal. Chem.* **1966**, *38*, 54.

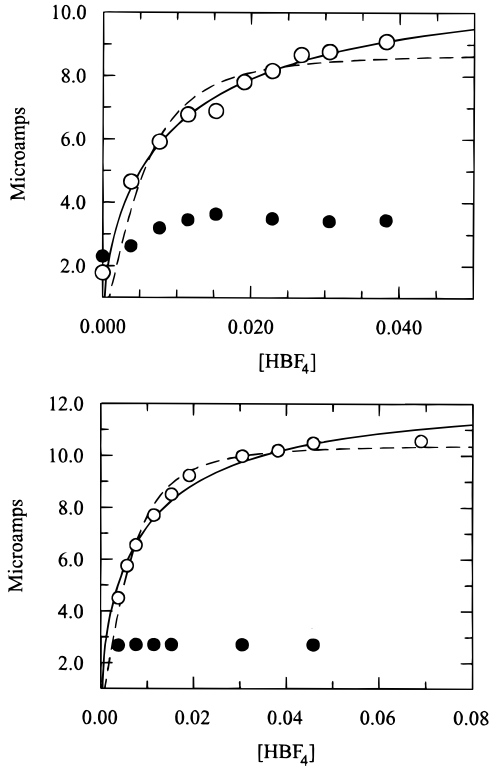

Figure 7. (Top) Dependence of the peak current on acid concentration for 2.30×10^{-3} M solutions of $[Pd(ttpE)(CH_3CN)](BF_4)_2$ saturated with nitrogen (solid circles) and carbon dioxide (open circles). All data were recorded at a scan rate of 0.05 V/s. The solid line shows the best-fit line using eq 7 with $k_1 = 22$ M^{-1} s^{-1} and $k_2 = 790$ M^{-1} s^{-1}. The dashed line represents the best-fit line assuming a second-order dependence on acid with $k_1 = 13$ M^{-1} s^{-1} and $k_2 = 7.7 \times 10^4$ M^{-2} s^{-1}. Because of the scan rate dependence of the peak current, k_1 and k_2 cannot be regarded as true rate constants, as discussed in the text. (Bottom) Dependence of the peak current on acid concentration for 1.90×10^{-3} M solutions of $[Pd(eptpE)(CH_3CN)](BF_4)_2$ saturated with nitrogen (solid circles) and carbon dioxide (open circles). All data were recorded at 0.05 V/s. The solid line shows the best-fit line using eq 7 with $k_1 = 43$ M^{-1} s^{-1} and $k_2 = 400$ M^{-1} s^{-1}. The dashed line represents the best-fit line assuming a second-order dependence on acid with $k_1 = 30$ M^{-1} s^{-1} and $k_2 = 6.3 \times 10^4$ M^{-2} s^{-1}. Because of the scan rate dependence of the peak current, k_1 and k_2 cannot be regarded as true rate constants, as discussed in the text.

centration and then becomes independent of it. This dependence is discussed in more detail below. The solid circles in Figure 7 show the currents observed for solutions of different acid concentrations in the absence of CO_2. At all acid concentrations, a significant current enhancement is observed for solutions purged with CO_2 compared to those purged with N_2. Plots of the catalytic current vs the square root of the CO_2 concentration and vs the catalyst concentration are shown in Figure 8 for compound **7a**. The square root dependence of the catalytic current on CO_2 concentration is consistent with a rate-determining step that is first order in CO_2.[24] The linear dependence of the current on catalyst concentration implies a first-order dependence on the catalyst concentration as well. The catalytic current of **8a** also shows a square root dependence on the CO_2 concentration and a linear dependence on catalyst concentration.

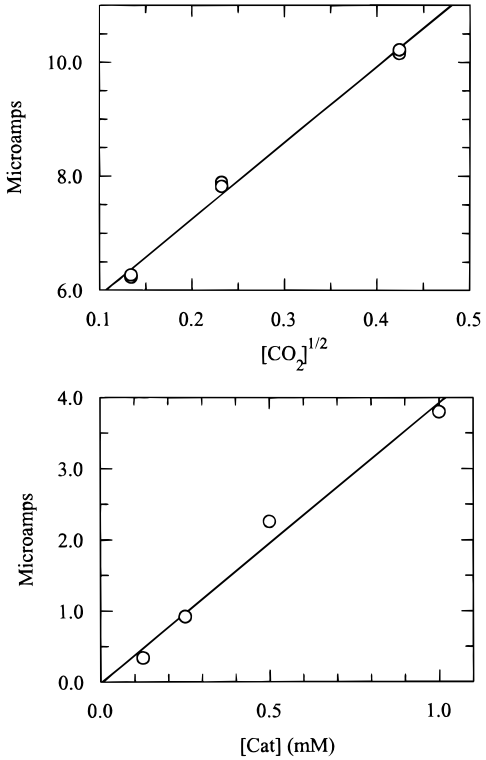

Figure 8. (Top) Dependence of the catalytic current on CO_2 concentration for a dimethylformamide solution containing 0.04 M HBF_4 and 2.30×10^{-3} M $[Pd(ttpE)(CH_3CN)](BF_4)_2$. The scan rate was 0.05 V/s. (Bottom) Dependence of the catalytic current on $[Pd(ttpE)(CH_3CN)](BF_4)_2$ concentrations for dimethylformamide solutions containing 0.04 M HBF_4 and 0.18 M CO_2. The scan rate was 0.1 V/s.

The catalytic current for **7a** was decreased 25−30% when the CO_2 pressure was held constant at 1 atm and the partial pressure of CO was increased to 0.5 atm and allowed to equilibrate for approximately 15 min. This indicates that the product, CO, inhibits its production. However, no evidence was observed by ^{31}P NMR spectroscopy for the reaction of **7a** with CO when an acidic dimethylformamide solution was saturated with CO at 1 atm. These results suggest that CO inhibition occurs by binding to reduced forms of the catalyst. Similar experiments were carried out with 0.25 atm of H_2. After equilibration for 15 min, no significant inhibition was observed.

Qualitative Molecular Orbital Calculations. Extended Hückel calculations were carried out for $[Pd(PH_3)_3]^{2+}$ and $[Pd(PH_3)_3H]^+$ to obtain a greater understanding of the influence of the chelate bite on the hydride complexes. Two parameter sets were used in these calculations and are listed in the Supporting Information. One was a relatively hard parameter set used by Thorn and Hoffmann for modeling olefin insertion reactions in Pt−H complexes.[5] The second parameter set was taken from the default values of a standard molecular modeling package.[25] Both parameter sets give the same trends. As the bond angle between the central phosphorus atom and the two terminal phosphorus atoms decreases from 100 to 80°, the calculated charge on the hydride ligand of $[Pd(PH_3)_3H]^+$ becomes more negative (−0.27 and −0.51, respectively, for the hard parameter set and −0.61 and −0.73, respectively,

(24) Savéant, J. M.; Vianello, E. *Electrochim. Acta* **1963**, *8*, 905.

(25) CAChe Scientific, Inc., 13475 SW Karl Braun, Beaverton, OR.

for the softer parameter set). This result implies that the hydridic nature of metal hydride complexes can be influenced by controlling the P−M−P bond angle. Hydride complexes with ligands that have small chelate bites should be more hydridic and less acidic than analogous complexes with ligands that have larger chelate bite sizes. The origin of this effect can be traced to the LUMO or $d_{x^2-y^2}$ orbital of the $[Pd(PH_3)_3]^{2+}$ fragment. This fragment orbital contains a significant contribution from the p_x orbital, which results in the polarization

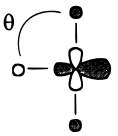

As the P−M−P angle (θ) increases, this orbital decreases in energy, causing electron density to move from the hydride ligand into this orbital. As a result, large P−M−P angles will produce more acidic hydrides. The lower energy of this orbital should also facilitate electron transfer from molecular hydrogen to this orbital, promoting heterolytic cleavage of hydrogen.

Discussion

A variety of new triphosphine ligands have been prepared which contain one, two, and three bridging methylene groups between the central and terminal phosphorus atoms of the triphosphine ligand. These ligands permit a systematic study of the effect of chelate bite size for triphosphine ligands on various properties of metal complexes. Because of our interest in CO_2 reduction by $[Pd(triphosphine)(CH_3CN)](BF_4)_2$ complexes, we have focused on palladium complexes of the type $[Pd(triphosphine)(CH_3CN)](BF_4)_2$, $[Pd(triphosphine)(PEt_3)](BF_4)_2$, and $[Pd(triphosphine)(H)](BF_4)$.

The reactions of $[Pd(NCCH_3)_4](BF_4)_2$ with triphosphine ligands containing two-carbon, three-carbon, and mixed two- and three-carbon chains result in the formation of mononuclear $[Pd(triphosphine)(CH_3CN)](BF_4)_2$ complexes (eq 4). The reaction of metpE, which contains a two-carbon and a one-carbon chain, with $[Pd(NCCH_3)_4](BF_4)_2$ in acetonitrile produces an equilibrium mixture of a monomeric (**12a**) and a dimeric species (**13a**) (eq 5). In the latter complex, the strained four-membered ring of the monomer has opened to form a bridge to a second palladium atom. This equilibrium can be shifted by varying the temperature and the solvent. The formation of such a dimeric species is not surprising, given the large number of dimeric species formed by ligands such as dppm with a methylene bridge between the phosphorus atoms.[26]

Reaction of the equilibrium mixture of **12a** and **13a** with $NaBH_4$ on alumina results in the clean and rapid formation of the Pd(I) dimer **14**, in which ring strain has been reduced by the formation of the larger five-membered rings upon Pd−Pd bond formation. The analogous reactions of the complexes **7a**−**9a** with $NaBH_4$ on alumina produce the corresponding hydrides. These results demonstrate that small chelate bites favor formation of Pd(I) dimers in the presence of $NaBH_4$ while large chelate bites promote hydride formation. The differences in the products formed in the reactions of the various triphosphine ligands with $[Pd(NCCH_3)_4](BF_4)_2$ and the products formed during the reaction of the $[Pd(triphosphine)(CH_3CN)](BF_4)_2$ complexes with $NaBH_4$ can be readily understood in terms of ring strain arguments.

There are other differences in the reactivity patterns of the mononuclear $[Pd(triphosphine)(CH_3CN)](BF_4)_2$ complexes containing two-carbon linkages compared to those with three-carbon chains which are not readily understood on the basis of differences in ring strain present in reduced intermediates. For example, the reaction of triethylphosphine with $[Pd(etpC)(CH_3CN)](BF_4)_2$ in noncoordinating solvents such as acetone produces the corresponding triethylphosphine complex $[Pd(etpC)(PEt_3)](BF_4)_2$, but $[Pd(ttpC)(CH_3CN)](BF_4)_2$ is unreactive with triethylphosphine under the same conditions. The rate of triethylphosphine exchange for $[Pd(ttpE)(PEt_3)](BF_4)_2$ with free triethylphosphine also appears to be more rapid than that of $[Pd(etpE)(PEt_3)](BF_4)_2$. In deuterionitromethane solutions containing 1 equiv of triethylphosphine, broad resonances are observed for the ^{31}P NMR spectrum of $[Pd(ttpE)(PEt_3)](BF_4)_2$ at room temperature, while the resonances of $[Pd(etpE)(PEt_3)](BF_4)_2$ are sharp. Excess triethylphosphine is required to obtain a fully reversible reduction wave for $[Pd(ttpE)(PEt_3)](BF_4)_2$, while no additional triethylphosphine is required to obtain reversible waves for $[Pd(etpE)(PEt_3)](BF_4)_2$ and $[Pd(eptpE)(PEt_3)](BF_4)_2$. This is consistent with triethylphosphine dissociation at low concentrations for the former complex but not for the latter complexes. A comparison of the X-ray crystal structures of $[Pd(MesetpE)(CH_3CN)](BF_4)_2$ and $[Pd(ttpE)(CH_3CN)](BF_4)_2$ is helpful in understanding these results. As can be seen from Figure 3, one of the methylene carbons of the two ethyl substituents on each terminal phosphorus atom of $[Pd(ttpE)(CH_3CN)](BF_4)_2$ has a close contact with the nitrogen atom of the acetonitrile ligand. This repulsive interaction would be expected to increase if the acetonitrile ligand is replaced with triethylphosphine and apparently becomes prohibitive for formation of the triethylphosphine complex $[Pd(ttpC)(PEt_3)](BF_4)_2$. The differences in the reactivity of the $[Pd(triphosphine)(CH_3CN)](BF_4)_2$ complexes with triethylphosphine are attributed to the steric interaction between triethylphosphine and the substituents on the terminal phosphorus atoms that lie along the acetonitrile axis.

The reaction of hydrogen with $[Pd(triphosphine)(S)](BF_4)_2$ complexes (where S is a weakly coordinating solvent such as DMF or acetone) is another reaction that exhibits a strong dependence on the chelate bite size. Only complexes with two trimethylene backbones have been observed to react with hydrogen to form the corresponding hydride, as shown in eq 6. One possible explanation for these differences is that the steric interaction observed in the formation of the triethylphosphine complexes also plays an important role in the formation of the hydride complex. Steric interactions between the coordinated solvent molecules and the terminal substituents in the $[Pd(triphosphine)(S)](BF_4)_2$

(26) (a) Puddephett, R. J. *Chem. Soc. Rev.* **1983**, *12*, 99. (b) Miedaner, A.; DuBois, D. L. *Inorg. Chem.* **1988**, *27*, 2479.

(27) (a) Baacke, M.; Hietkamp, S.; Morton, S.; Stelzer, O. *Chem. Ber.* **1981**, *114*, 2568. (b) Miedaner, A.; Curtis, C. J.; Barkley, R. M.; DuBois, D. L. *Inorg. Chem.* **1994**, *33*, 5482. (c) King, R. B.; Cloyd, J. C., Jr. *J. Am. Chem. Soc.* **1975**, *97*, 46.

complexes with trimethylene chains could be significant and destabilize the reactants by weakening the Pd−S bond. These steric interactions would be expected to be less important for the products, $[Pd(ttpE)(H)](BF_4)$ and $[Pd(ttpC)(H)](BF_4)$, because of the smaller steric requirements of the hydride ligand. These considerations would suggest that steric interactions should favor formation of the hydride complexes for complexes with three-carbon chains. The lower energy of the LUMO or $d_{x^2-y^2}$ orbital for large P−M−P angles indicates that there is also an electronic component that favors hydride formation.

A second interesting aspect of the hydride complexes, suggested by the molecular orbital calculations discussed above, is the possibility of using the chelate bite size to partially control the hydridic character of the hydride ligand. The smaller the P−M−P bond angle, the more hydridic the hydride ligand should become, whereas larger bond angles favor more acidic hydride ligands. In our hands, the addition of HBF_4 to dimethylformamide solutions of $[Pd(etpC)(H)](BF_4)$, which contains five-membered chelate rings, results in the rapid evolution of H_2 and the formation of $[Pd(etpC)(DMF)](BF_4)_2$. For $[Pd(ttpC)(H)](BF_4)$, no reaction is observed under these conditions. Similarly, many square-planar hydrides are synthesized by protonation of zerovalent metal complexes using weak to strong acids.[20,28] The complex $[(PPh_3)_3PdH]^+$ is relatively stable in aqueous solutions containing up to 80% CF_3COOH,[29] and the hydride ligand in *trans*-$[(Cy_3P)_2Pd(H)(H_2O)]^+$ exchanges more rapidly with D_2O than the protons bound to coordinated water.[20b] These results are consistent with acidic hydride complexes. The average O−Pd−P bond angle in the latter complex is approximately 95°. An even larger angle would be expected for $[(PPh_3)_3PdH]^+$.

Electrocatalytic Reduction of CO_2. The increased catalytic current observed in the presence of CO_2 for acidic dimethylformamide solutions of $[Pd(ttpE)(CH_3CN)]^{2+}$ (**7a**) suggested that this compound catalyzes the electrochemical reduction of CO_2 (Figure 5, traces c and d). This was confirmed by controlled-potential electrolysis experiments carried out at −1.4 V and identification of CO as the major reduction product by gas chromatography. Similar results were obtained for $[Pd(eptpE)(CH_3CN)]^{2+}$ (**9a**). The dependence of the catalytic current on acid concentration for **7a** and **9a** (Figure 7) is consistent with two different rate-determining steps. At low acid concentrations, the catalytic current is dependent on the acid concentration, but at higher acid concentrations, no dependence is observed. The best-fit line of these data using eq 7 is shown by the

$$\frac{i_c}{i_d} = \frac{\sigma}{0.447}\left(\frac{RT}{nFv}\right)^{1/2}\left(\frac{k_1k_2[CO_2][H^+]}{k_1[CO_2] + k_2[H^+]}\right)^{1/2} \qquad (7)$$

solid curves in Figure 7. In eq 7, i_c is the catalytic current, i_d is the peak current due to reversible reduction of the catalyst, v is the scan rate, n is the number of electrons involved in catalyst reduction, k_1 and k_2 are rate constants for the two rate-determining steps discussed below, and σ is a factor that depends on whether the electron transfer to the catalyst occurs at the electrode surface or in solution. Equation 7 assumes a first-order dependence of the catalytic rate on acid at low acid concentrations and first-order dependence on CO_2 at high acid concentrations. For $[Pd(triphosphine)(CH_3CN)](BF_4)_2$ complexes containing triphosphine ligands with two ethylene bridges, two rate-determining steps are also observed. For the ethylene-bridged complexes, a second-order dependence of the catalytic rate on acid concentration has been observed for several catalysts at low acid concentrations and a first-order dependence on CO_2 at high acid concentrations.[10,11] These results suggest that the rate-determining step for the reduction of CO_2 is the same at high acid concentrations for $[Pd(ttpE)(CH_3CN)](BF_4)_2$, $[Pd(eptpE)(CH_3CN)](BF_4)_2$, and the catalysts with two-carbon-chain backbones. This step has been proposed previously to be the reaction of a Pd(I) intermediate with CO_2 as shown in eq 8. This is consistent with the one-electron reduction

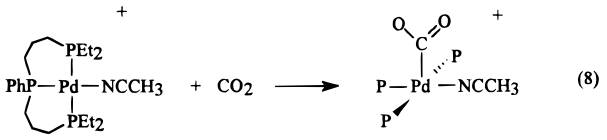

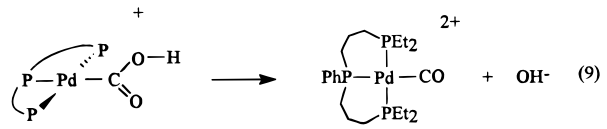

observed for $[Pd(ttpE)(CH_3CN)](BF_4)_2$ in the presence of CO_2, as discussed above in the Results Section. At low acid concentrations, there appears to be a subtle difference in the mechanism of the rate-determining step. For the top graph of Figure 7, it can be seen that the data are best fit by the solid line, which corresponds to a first-order dependence on acid at low acid concentrations. The dotted line, which corresponds to a second-order dependence on acid, does not fit as well. The first-order dependence of the catalytic rate on acid observed for $[Pd(ttpE)(CH_3CN)](BF_4)_2$ suggests loss of hydroxide from the activated complex as shown in eq 9, whereas the second-order dependence observed for catalysts containing ethylene linkages is consistent with loss of water. Precedents for both pathways exist in the literature.[30−32] The greater steric interaction between the ethyl substituents on the terminal phosphorus atoms and the hydroxycarbonyl ligand should promote loss of hydroxide from $[Pd(ttpE)(COOH)]^+$. There are steps in addition to eqs 8 and 9 that must occur during the catalytic reduction of CO_2 to CO by $[Pd(triphosphine)(CH_3CN)](BF_4)_2$ complexes. An electron transfer precedes reaction 8, and a second electron transfer, protonation, and solvent loss occur between steps 8 and 9. Following reaction 9, CO must be replaced by a solvent molecule to regenerate a $[Pd(triphosphine)-$

(28) (a) Gerlach, D. H.; Kane, A. R.; Parshall, G. W.; Jesson, J. P.; Muetterties, E. L. *J. Am. Chem. Soc.* **1971**, 3544. (b) Siedle, A. R.; Newmark, R. A.; Gleason, W. B. *Inorg. Chem.* **1991**, *30*, 2005. (c) Seligson, A. L.; Cowan, R. L.; Trogler, W. C. *Inorg. Chem.* **1991**, *30*, 3371.

(29) (a) Zudin, V. N.; Chinakov, V. D.; Nekipelov, V. M.; Rogov, V. A.; Likholobov, V. A.; Yermakov, Y. I. *J. Mol. Catal.* **1989**, *52*, 27. (b) Zudin, V. N.; Chinakov, V. D.; Nekipelov, V. M.; Likholobov, V. A.; Yermakov, Y. I. *J. Organomet. Chem.* **1985**, *289*, 425.

(30) (a) Byrd, J. E.; Halpern, J. *J. Am. Chem. Soc.* **1971**, *93*, 1634. (b) Catellani, M.; Halpern, J. *Inorg. Chem.* **1980**, *19*, 566.

(31) Bennett, M. A.; Robertson, G. B.; Rokicki, A.; Wickramasinghe, W. A. *J. Am. Chem. Soc.* **1988**, *110*, 7098.

(32) Ford, P. C.; Rokicki, A. *Adv. Organomet. Chem.* **1988**, *28*, 139.

(solvent)]$^{2+}$ species, which is reduced to start the next catalytic cycle. Evidence for these reactions has been presented previously and is not repeated here.[10] However, steps 8 and 9 are rate-determining and therefore control the kinetic behavior of [Pd(ttpE)(CH_3CN)](BF_4)$_2$.

[Pd(eptpE)(CH_3CN)](BF_4)$_2$, which contains both trimethylene and ethylene bridges in the triphosphine ligand, appears to exhibit behavior midway between that expected for complexes containing two ethylene or two trimethylene linkages. As shown by the bottom graph of Figure 7, the catalytic current appears to fall between the best-fit curves for first- and second-order acid dependence. This may indicate that both pathways are available to this catalyst. At high acid concentrations, the catalytic rate is first order in CO_2 and catalyst, as previously observed for complexes with two ethylene linkages.

Ideally, the catalytic current should not depend on the scan rate.[22] However, that is not true for complexes **7a**−**9a**, perhaps due to product inhibition by CO or to rapid catalyst decomposition. Because of this behavior, it is not meaningful to compare the catalytic rates of these complexes to those of their two-carbon-chain analogues reported earlier.[10,11] It is interesting, however, to compare the decomposition products formed during the catalytic process. The electrochemical reduction of [Pd(etpE)(CH_3CN)](BF_4)$_2$, [Pd(eptpE)(CH_3CN)](BF_4)$_2$, [Pd(ttpE)(CH_3CN)](BF_4)$_2$, and [Pd(ttpC)(CH_3CN)](BF_4)$_2$ in the presence of CO_2 leads to the formation of [Pd(etpE)]$_2$(BF_4)$_2$, [Pd(eptpE)(H)](BF_4), [Pd(ttpE)(H)](BF_4), and [Pd(ttpC)(H)](BF_4), respectively, as the major products. These are the same products that are observed by ^{31}P NMR spectroscopy of the crude reaction mixtures at the end of catalytic experiments. Increasing the chain length of the triphosphine ligand from two carbons to three carbons apparently prevents dimer formation, but a new decomposition pathway that involves abstraction of a hydrogen atom from the reaction medium becomes dominant. Due to the stability of the hydride complexes containing three-carbon chains in acidic media, hydride formation constitutes an effective decomposition pathway. The stability of the hydrides containing trimethylene linkages under relatively acidic solutions and their formation by direct heterolytic cleavage of hydrogen suggest that these complexes may have other interesting catalytic properties. This area will be the subject of future studies.

Summary and Conclusions

One of the original objectives of this work was to prepare [Pd(triphosphine)(CH_3CN)](BF_4)$_2$ complexes in which the triphosphine ligand contained two trimethylene chains. It was felt that such complexes would prevent the formation of Pd(I) dimers of type **1** that were observed as the decomposition products during the electrochemical reduction of CO_2 catalyzed by [Pd(triphosphine)(CH_3CN)](BF_4)$_2$ complexes with two ethylene bridges. Although dimer formation was not found to be a major decomposition pathway for the complexes containing two trimethylene bridges, catalyst lifetime was not significantly improved, since a new decomposition pathway, the formation of [Pd(triphosphine)(H)](BF_4) complexes, emerged to replace it.

As expected, the tendency to form bridged complexes is greater for the triphosphine ligands with smaller chelate bites. The ligand containing one ethylene and one methylene backbone, metpE, forms bridged, dimeric complexes for Pd(II) and Pd(I) oxidation states. For ligands with two ethylene backbones, bridged complexes are not observed for the Pd(II) oxidation state, but Pd(I) dimers are formed readily during electrochemical reductions. For complexes containing two trimethylene backbones, hydride species are formed exclusively under similar conditions.

Crystal structures of [Pd(ttpE)(CH_3CN)](BF_4)$_2$ and [Pd(ttpE)(H)](BF_4) indicate that a significant steric interaction exists between the substituents on the terminal phosphorus atoms of the triphosphine ligand and the fourth ligand in square-planar complexes. This steric interaction undoubtedly plays a significant role in the failure of [Pd(ttpC)(CH_3CN)](BF_4)$_2$ to coordinate triethylphosphine. Formation of the hydrides [Pd(ttpE)(H)](BF_4) and [Pd(ttpC)(H)](BF_4) from the analogous solvent complexes is also favored by weakening the Pd−S bond. Finally, this steric interaction promotes the loss of hydroxide from the hydroxycarbonyl complex formed during electrochemical reduction of CO_2 to CO. In the analogous ethylene-bridged complexes, water is lost rather than hydroxide.

The larger bite size of the complexes with trimethylene linkages also produces an electronic stabilization of the hydride complexes compared to their two-carbon-chain analogues. This suggests the possibility of using chelating ligands with large bite sizes as a strategy for promoting heterolytic cleavage of hydrogen by complexes containing weakly coordinating solvent molecules. This aspect will be pursued in future work. In addition, the qualitative molecular orbital calculations used here indicate that the chelate bite can be used to modulate the charge associated with hydride ligands.

Experimental Section

Materials and Physical Methods. Details of methods used for drying solvents, spectral measurements, and gas chromatography experiments have been presented elsewhere.[10,11] Elemental analyses were performed by Schwarzkopf Microanalytical Laboratory, Inc. The following reagents were purchased from commercial suppliers and used as obtained: allylmagnesium chloride, vinylmagnesium bromide, phenylphosphine, chlorodiethylphosphine, $NaBH_4$ supported on basic alumina, triethylphosphine, butyllithium, and 2,2′-azobis(2-methylproprionitrile) (AIBN). Bis(3-(dicyclohexylphosphino)propyl)phenylphosphine (ttpC),[15a] [Pd($NCCH_3$)$_4$](BF_4)$_2$,[33] diethylvinylphosphine,[34] (chloromethyl)diphenylphosphine,[13] and [Pd(etpC)(CH_3CN)](BF_4)$_2$[10] were prepared according to literature methods.

Coulometric measurements were carried out at 25−30 °C using a Princeton Applied Research Model 173 potentiostat equipped with a Model 179 digital coulometer and a Model 175 universal programmer. The working electrode was constructed from a reticulated vitreous carbon rod with a diameter of 1 cm and length of 2.5 cm (60 pores per inch, The Electrosynthesis Co., Inc.), the counter electrode was a Pt wire, and a Ag wire immersed in a permethylferrocene/permethylferrocenium solution was used as the pseudoreference electrode.[35] The electrode compartments were separated by Vycor disks (7 mm diameter, EG&G Princeton Applied Research).

(33) (a) Sen, A.; Ta-Wang, L. *J. Am. Chem. Soc.* **1981**, *103*, 4627. (b) Hathaway, B. J.; Holah, D. G.; Underhill, A. E. *J. Chem. Soc.* **1962**, 2444.

(34) Askham, F. R.; Stanley, G. G.; Marques, E. C. *J. Am. Chem. Soc.* **1985**, *107*, 7423.

(35) Bashkin, J. K.; Kinlen, P. J. *Inorg. Chem.* **1990**, *29*, 4507.

Measurements of current efficiencies for gas evolution were carried out in a sealed flask from which aliquots were removed for GC analysis. Catalytic coulometric experiments were considered complete when the current had decayed to 5−10% of its original value in the presence of 0.18 M CO_2 and 0.1 M HBF_4, i.e., the same as the initial conditions. Cyclic voltammetry and chronoamperometry experiments were carried out using a Cypress System computer-aided electrolysis system at 21 ± 0.5 °C unless stated otherwise. The working electrode was a glassy-carbon electrode (Cypress Systems, Inc.). Ferrocene was used as an internal standard, and all potentials are reported vs the ferrocene/ferrocenium couple.[36] The solubility of CO_2 in dimethylformamide was taken from ref 37. All solutions for CV and coulometric experiments were 0.3 N NEt_4BF_4 in dimethylformamide unless otherwise stated. FAB mass spectra were recorded on a VG Analytical 7070 EQ-HF tandem mass spectrometer. Samples were dissolved in nitrobenzyl alcohol (NOBA).

Syntheses. Allyldiethylphosphine.[38] A 500 mL three-necked flask was fitted with an N_2 inlet, mechanical stirrer, and 250 mL addition funnel. PEt_2Cl (30 g, 0.24 mol) was transferred by cannula to the flask, dissolved in 150 mL of THF, and cooled to −80 °C. Allylmagnesium chloride (120 mL of a 2 M solution in THF, 0.24 mol) was transferred by cannula to the addition funnel and added dropwise over 1 h to the phosphine solution. After complete addition, the slurry of a white precipitate in a pale gray solution was warmed to room temperature and stirred for 2 h. The volatile components were transferred under vacuum, and the product was collected by fractional distillation (138−140 °C/615 mmHg) as a clear, colorless liquid (24.7 g, 78%). ^{1}H NMR (toluene-d_8): δ 5.69 (m, 1H, CH_2=C*H*); 4.93 (m, 2H, C*H*$_2$=CH); 2.04 (d, 2H, CH−C*H*$_2$P); 1.20 (m, 4H, C*H*$_2$CH$_3$); 0.96 (m, 6H, CH_2C*H*$_3$). ^{31}P-{^{1}H} NMR (toluene-d_8): −23.7 ppm (s).

Bis(3-(diethylphosphino)propyl)phenylphosphine (ttpE; 2). A mixture of allyldiethylphosphine (4.72 g, 36 mmol), phenylphosphine (2.0 g, 18 mmol), and AIBN (100 mg) was irradiated in a sealed Schlenk flask using a Rayonet photoreactor with 254 and 350 nm lamps for 4.5 days. Volatile materials were removed under vacuum at 150 °C for 2 h. The crude, yellow oil (3.2 g, 48%) was distilled under vacuum (175 °C/0.1 mmHg). A similar procedure was used to prepare bis-(3-(dicyclohexylphosphino)propyl)phenylphosphine (**3**). In this case, the ligand could not be distilled, but its spectral parameters are identical with those reported using a different synthetic route.[15a]

(2-(Diethylphosphino)ethyl)phenylphosphine (4). A mixture of phenylphosphine (25 g, 0.227 mol), diethylvinylphosphine (6 g, 0.052 mol), and AIBN (100 mg) was irradiated for 19 h in a sealed Schlenk flask using a Rayonet photoreactor with 254 and 350 nm bulbs. The crude mixture was fractionally distilled to separate unreacted phenylphosphine. The product was isolated as a clear oil (9.5 g, 81%). ^{1}H NMR (toluene-d_8): δ 7.34, 7.04 (m, 5H, Ph); 4.14 (dt, 1H, PH, $^1J_{PH}$ = 204 Hz, J_{HH} = 7 Hz); 1.73 (m, 2H, CH_2); 1.36 (m, 2H, CH_2); 1.11 (m, 4H, C*H*$_2$CH$_3$); 0.89 (m, 6H, CH_2C*H*$_3$). ^{31}P{^{1}H} NMR (toluene-d_8): −19.9 ppm (d, Et_2P, $^3J_{PP}$ = 17.1 Hz), −45.5 ppm (d, PhP).

Lithium (2-(Diethylphosphino)ethyl)phenylphosphide. (2-(Diethylphosphino)ethyl)phenylphosphine (4.0 g, 0.018 mol) was dissolved in hexane (30 mL) and cooled to −78 °C. Butyllithium (7 mL, 0.02 mol) was added slowly by syringe. After complete addition, the solution was warmed to room temperature and stirred for 2 h. The hexane supernatant was removed by cannula and the remaining yellow solid (4.1 g, 98%) was washed with hexane (2 × 30 mL) and dried in vacuo for 1 h. *Caution!* This compound is pyrophoric. ^{1}H NMR (THF-d_8): δ 6.2−7.5 (br m, 5H, Ph); 1.9 (br s, 2H, CH_2); 1.6 (br s, 2H, CH_2); 1.4 (m, 4H, C*H*$_2$CH$_3$); 1.0 (m, 6H, CH_2C*H*$_3$). ^{31}P{^{1}H} NMR (THF-d_8): −22.7 ppm (d, Et_2P, ^3J = 13.4 Hz), −40.1 ppm (br, PhP).

(2-(Diethylphosphino)ethyl)(3-(diethylphosphino)-propyl)phenylphosphine (eptpE; 5). A mixture of (2-(diethylphosphino)ethyl)phenylphosphine (**4**; 4.5 g, 0.02 mol), allyldiethylphosphine (2.6 g, 0.02 mol), and AIBN (100 mg) was irradiated for 1.5 days in a sealed Schlenk flask, as described above. The crude product was distilled at 163−165 °C at reduced pressure (0.01 mmHg) to obtain a clear, pale yellow oil (5.4 g, 76%).

(2-(Diethylphosphino)ethyl)((diphenylphosphino)-methyl)phenylphosphine (metpE; 6). A −78 °C THF solution of lithium (2-(diethylphosphino)ethyl)phenylphosphide (3.0 g, 13 mmol) was transferred slowly by cannula to a −78 °C THF solution of (chloromethyl)diphenylphosphine (3.03 g, 13 mmol). After complete addition, the solution was warmed to room temperature and stirred for 15 h. The solvent was removed under vacuum, and the resultant oil was dissolved in 40 mL of an acetone/ethanol (1:1) mixture. The solution was concentrated to 25 mL and placed in a −10 °C freezer for 3 days. A viscous oil formed on the bottom of the flask. The supernatant was removed by cannula, and the oil was washed with degassed H_2O (2 × 20 mL) and extracted with Et_2O (30 mL). The ether was stripped under vacuum, leaving a viscous, yellow oil (4.17 g, 87.1%). The ligand was used without further purification.

[Pd(ttpE)(NCCH$_3$)](BF$_4$)$_2$ (7a(BF$_4$)$_2$). [Pd(NCCH$_3$)$_4$](BF$_4$)$_2$ (0.77 g, 1.7 mmol) and ttpE (0.68 g, 1.8 mmol) were dissolved in CH_3CN (20 mL). After it was stirred for 30 min, the solution was concentrated to 10 mL and layered with Et_2O (30 mL). After a yellow solid precipitated, the supernatant was removed by cannula. The solid (1.2 g, 97%) was dried under vacuum at 50 °C for 1 h. The crude product can be recrystallized from a dichloromethane/ethanol mixture containing 5% acetonitrile. Anal. Calcd for $C_{22}H_{40}NB_2F_8P_3Pd$: C, 38.21; H, 5.83; N, 2.03. Found: C, 37.62; H, 5.93; N, 1.82. ^{1}H NMR (CD_3CN): δ 7.65−7.90 (m, 5H, Ph); 2.42, 2.2, 2.1, 1.75, 1.20 (complex multiplets, C_2H_5 and $(CH_2)_3$). IR (Nujol mull): ν_{CN} 2321 and 2292 cm^{-1}. Addition of acetonitrile (2.5 μL) to a solution of **7a** (20 mg) in acetone-d_6 resulted in a shift of the resonance assigned to acetonitrile from 2.7 to 2.2 ppm.

[Pd(ttpC)(CH$_3$CN)](BF$_4$)$_2$ (8a(BF$_4$)$_2$), [Pd(eptpE)-(CH$_3$CN)](BF$_4$)$_2$ (9a(BF$_4$)$_2$), and [Pd(metpE)(CH$_3$CN)]-(BF$_4$)$_2$ (12a(BF$_4$)$_2$), and [Pd(metpE)L]$_2$(BF$_4$)$_4$ (13(BF$_4$)$_4$). These complexes were prepared in a manner analogous to that used for **7a**. All of these complexes gave satisfactory analyses, as shown by the following example. Anal. Calcd for [Pd-(metpE)(CH$_3$CN)]$_n$(BF$_4$)$_{2n}$, $C_{27}H_{34}NB_2F_8P_3Pd$: C, 43.48; H, 4.60; N, 1.88. Found: C, 43.73; H, 4.82; N, 2.01. In acetonitrile-d_3, both monomeric (**12a**) and dimeric (**13a**) species are observed by ^{31}P NMR spectroscopy. Spectral data for **12a** are given in Table 1. Parameters used for simulating the ^{31}P NMR spectrum of **13a** (Figure 1) are as follows: 98.57 ppm, P_A; 9.26 ppm, P_B; 62.37 ppm, P_X; −337 Hz, J_{AB}; 0.0 Hz, $J_{AB'}$; 2.0 Hz, J_{AX}; 0.0 Hz, $J_{AX'}$; −31.28 Hz, J_{BX}; 16.99 Hz, $J_{BX'}$; 8.50 Hz, $J_{BB'}$. If this compound is isolated from acetone solutions with no added acetonitrile, dimer **13b** or **13c**, where L is acetone, is observed by ^{31}P NMR. Parameters for simulation of this spectrum are as follows: 75.01 ppm, P_A; 9.74 ppm, P_B; 64.24 ppm, P_X; 25.0 Hz, J_{AB}; 0.0 Hz, $J_{AB'}$; 5.04 Hz, J_{AX}; −0.17 Hz, $J_{AX'}$; 397 Hz, J_{BX}; 16.39 Hz, $J_{BX'}$. The experimental and simulated spectra are shown in Figure 3s of the Supporting Information.

[Pd(eptpE)(PEt$_3$)](BF$_4$)$_2$ (9b(BF$_4$)$_2$). Triethylphosphine (122 μL, 0.82 mmol) was added via syringe to a solution of [Pd(eptpE)(NCCH$_3$)](BF$_4$)$_2$ (0.508 g, 0.75 mmol) in CH_3CN (30 mL). After the reaction mixture was stirred for 30 min, 30 mL of ethanol was added by cannula, and the volume was

(36) (a) Gagné, R. R.; Koval, C. A.; Lisensky, G. C. *Inorg. Chem.* **1980**, *19*, 2854. (b) Gritzner, G.; Kuta, J. *Pure Appl. Chem.* **1984**, *56*, 462. (c) Hupp, J. T. *Inorg. Chem.* **1990**, *29*, 5010.

(37) Stephen, H., Stephen, T., Eds. *Solubilities of Inorganic and Organic Compounds*; Pergamon Press: New York, 1958; Vol. 1, p 1063.

(38) Hewertson, W. German Patent 2057771 710603, 1991; *Chem. Abstr.* **1971**, *75*, 49333y.

Table 4. Crystal Data, Data Collection Conditions, and Solution Refinement Details for [Pd(ttpE)(CH$_3$CN)](BF$_4$)$_2$ (7a(BF$_4$)$_2$) and [Pd(ttpE)(H)](BF$_4$) (7c(BF$_4$))

	7a(BF$_4$)$_2$	**7c**(BF$_4$)
empirical formula	$C_{22.125}H_{40.25}B_2Cl_{0.25}F_8NP_3Pd$	$C_{20}H_{38}BF_4P_3Pd$
color, habit	colorless block	pale yellow wedge
space group	*C*2/*c*	$P\bar{1}$
cryst syst	monoclinic	triclinic
a, Å	27.505(6)	8.217(2)
b, Å	9.112(2)	12.330(3)
c, Å	26.749(5)	12.794(3)
α, deg	90	94.64(3)
β, deg	101.57(3)	100.01(3)
γ, deg	90	107.29(3)
V, Å^3	6568(2)	1206.6(4)
Z	8	2
d_{calcd}, g/cm^3	1.420	1.554
fw	702.1	564.6
abs coeff, mm^{-1}	0.790	1.004
radiation	Mo Kα (*λ* = 0.710 73 Å)	Mo Kα (*λ* = 0.710 73 Å)
temp, K	178	178
final *R* indices ($I > 2\sigma(I)$)[a]	R1 = 0.0627, wR2 = 0.1678	R1 = 0.0282, wR2 = 0.0630
R indices (all data)[a]	R1 = 0.1035, wR2 = 0.1891	R1 = 0.0348, wR2 = 0.0657
no. of data/restraints/params	7277/0/341	5649/220/292
no. of rflns obsd	4517	4925

[a] $R1 = \sum||F_o| - |F_c||/\sum|F_o|$; $wR2 = [\sum[w(F_o^2 - F_c^2)]/\sum[w(F_o^2)^2]]^{1/2}$.

reduced under vacuum to 30 mL. The resulting yellow powder (0.38 g, 51%) was collected by filtration and dried under vacuum at 50 °C for 1 h. Anal. Calcd for $C_{25}H_{50}B_2F_8P_4Pd$: C, 39.79; H, 6.68; P, 16.42. Found: C, 39.71; H, 6.82; P, 15.35. A similar procedure was used to prepare [Pd(etpC)(PEt$_3$)](BF$_4$)$_2$ and [Pd(ttpE)(PEt$_3$)](BF$_4$)$_2$, but dichloromethane was used as the solvent. We were unable to prepare the analogous [Pd(eptpC)(PEt$_3$)](BF$_4$)$_2$ complex.

[Pd(ttpE)(H)](BF$_4$) (7c(BF$_4$)). [Pd(ttpE)(NCCH$_3$)](BF$_4$)$_2$ (0.72 g, 1.04 mmol) and NaBH$_4$ supported on alumina (~10% by weight, 0.421 g, 1.12 mmol) were slurried in 25 mL of CH$_3$CN. After it was stirred for 30 min, the solution was filtered, concentrated to ~10 mL, and layered with Et$_2$O (30 mL). The resulting solid (0.43 g, 73%) was collected by filtration, washed with degassed H$_2$O (25 mL), and dried in vacuo for 4 h. Crystals were grown from a mixture of acetone and ethanol at −20 °C. Anal. Calcd for $C_{20}H_{38}BF_4P_3Pd$: C, 42.54; H, 6.78; P, 16.46. Found: C, 43.25; H, 7.00; P, 15.27. Similar procedures were used to prepare [Pd(ttpC)(H)](BF$_4$) (**8c**(BF$_4$)), [Pd(eptpE)(H)](BF$_4$) (**9c**(BF$_4$)), and [Pd(etpC)(H)](BF$_4$) (**11c**(BF$_4$)).

[Pd(metpE)]$_2$(BF$_4$)$_2$ (14(BF$_4$)$_2$). NaBH$_4$ on alumina (200 mg) was added to a solution of [Pd(metpE)(CH$_3$CN)](BF$_4$)$_2$ (0.25 g, 0.34 mmol) in acetonitrile (20 mL). The solution immediately turned orange-brown. The reaction mixture was stirred for 15 min and the solvent removed with a vacuum. Dichloromethane (20 mL) was added to the residue, and the resulting slurry was filtered to remove excess NaBH$_4$/alumina. Ethanol (20 mL) was added to the filtrate, and the volume of the solution was reduced to approximately 7 mL. Upon standing overnight, a precipitate formed. The orange-brown solid (0.104 g, 51%) was collected by filtration and dried under vacuum at 55 °C for 3 h. Anal. Calcd for $C_{50}H_{62}P_6Pd_2B_2F_8$: C, 48.62; H, 5.06. Found: C, 48.52; H, 4.91. ^{31}P NMR (acetonitrile-d_3): second-order spectrum with complex multiplets at 53.4 (P_A), 35.9 (P_M), and −8.0 ppm (P_X). *N* values: N_{AM} = 5 Hz; N_{AX} = 14 Hz; N_{MX} = 420 Hz. FAB mass spectrum (NOBA): parent ion minus BF$_4^-$, *m*/*z* 1149; parent ion minus H(BF$_4$)$_2^-$, *m*/*z* 1061. Complex isotopic patterns match those calculated for a dimer with two Pd atoms. Electrospray mass spectrometry also gave ion peaks with maxima at *m*/*z* 1149 and 1061.

X-ray Diffraction Studies. A crystal of [Pd(ttpE)(CH$_3$CN)](BF$_4$)$_2$·0.125CH$_2$Cl$_2$ was selected under Exxon Paratone N oil, mounted with a small amount of silicone grease, and placed under a cold stream of N$_2$ (153 K) for data collection. Similarly, crystals of [Pd(ttpE)(H)](BF$_4$) were examined at low temperature, approximately 210 K, under Paratone N oil. A suitable crystal was selected and mounted under a cold stream of N$_2$ (178 K). Data were collected on a Siemens P3/F autodiffractometer. Mo Kα radiation (monochromatized by diffraction off a highly oriented graphite crystal) was used in this study. Programs in the Siemens X-ray package was used for data collection and for structure solution and refinement. Details of the experimental conditions are given in the Supporting Information. Table 4 summarizes the crystal data for [Pd(ttpE)(CH$_3$CN)](BF$_4$)$_2$ and [Pd(ttpE)(H)](BF$_4$).

Acknowledgment. This work was supported by the United States Department of Energy, Office of Basic Energy Sciences, Chemical Sciences Division.

Supporting Information Available: Tables 1s−16s, containing crystal data, data collection conditions, solution and refinement details, atomic coordinates and equivalent isotropic displacement parameters, bond lengths, bond angles, anisotropic displacement parameters, and hydrogen atom coordinates and isotropic parameters for **7a** and **7c**, Table 17s, giving parameters used in extended Hückel calculations, and Figure 3s, showing experimental and calculated ^{31}P NMR spectra for **13b** or **13c** (22 pages). Ordering information is given on any current masthead page.

OM960072S